NTNU – Trondheim
Norwegian University of
Science and Technology

Stress measurements in landfast sea ice in Van Mijenfjorden,Svalbard.

A survey of internal stress in landfast sea ice
winter 2014.

Carl Magnus Vindegg

Civil and Environmental Engineering
Submission date: June 2014
Supervisor: Amund Bruland, BAT
Co-supervisor: Aleksey Marchenko, UNIS

Norwegian University of Science and Technology
Department of Civil and Transport Engineering

NORWEGIAN UNIVERSITY OF SCIENCE AND TECHNOLOGY
DEPARTMENT OF CIVIL AND TRANSPORT ENGINEERING

Report Title: Stress measurements in landfast sea ice in Van Mijenfjorden in Svalbard.	Date:21.06.2014 Number of pages (incl. appendices): 73			
	Master Thesis	x	Project Work	

Name:
Carl Magnus Vindegg

Professor in charge/supervisor:
Amund Bruland

Other external professional contacts/supervisors:
Knut V. Høyland, Aleksey Marchenko

Abstract:

During the winter 2014 a fieldwork was conducted in Van Mijenfjorden, Svalbard. The main objective of the fieldwork was to investigate stress development in confined landfast ice. It was recorded maximum stress of 162 kPa close to a hinge zone. Bending of the ice contributed strongly to stress development. The direction of the stress was parallell to the shore. The maximum stress 200 meters further out was 37.7 kPa. This event correlated with a temperature increase at the ice surface. The stress was significantly higher close to the hinge zone than 200 meters. Stress correlated well with the tidal cyclus.

Keywords:

1. Sea ice
2. Stress
3. Landfast ice
4.

Acknowledgement

I would like to use this opportunity to thank my two partners in crime during a long and cold fieldwork campaign at Svea David Wrangborg and Bård Blæsterdalen. Thank you for exiciting and character-building hours at Barryneset and Fabrice cabin. I will thank prof. Knut Vilhelm Høyland and prof. Aleksey Marchenko for guidance and help. Store Norske Spitsbergen Grubekompani deserve acknowledgment for the great food and accomodation in Svea during the winter. The University Center in Svalbard with all the students and employers must be thanked for keeping an easy mind and low shoulders. Last but not least must Svalbard Villmarkssenter with the 8 maniacs be thanked for an unforgettable winter at Svalbard.

Summary

During the winter 2014 a fieldwork was conducted in Van Mijenfjorden, Svalbard. The main objective of the fieldwork was to investigate stress development in confined landfast ice. Investigation were performed at two sites: on the landfast ice close to a hinge zone and on the landfast ice 200 meters from shore. Three stress sensors were installed in a rosette with a fourth sensor at a different depth to observe the stress distribution in the ice at each site. Tiltmeters measured inclination of the ice at both sites. It was recorded maximum stress of 162 kPa close to the hinge zone. In addition were 4 stress peaks over 90 kPa registred. Bending of the ice contributed strongly to stress development. The direction of the stress was parallell with the shore. The maximum stress 200 meters further out was 37.7 kPa. This event correlated with a temperature increase of the ice surface which most likely was due to flooding. The stress was significantly higher close to the hinge zone than 200 meters further out through the season. Stress at both sites correlated well with the tidal cyclus. Stress close to the shore was highest at low tide, and stress 200 meters further out was highest at high tide.

Sammendrag

Vinteren 2014 ble et feltarbeid gjennomført i Van Mijenfjorden, Svalbard. Hensikten med feltarbeidet var å studere trykkgenerasjon i innestengt sjøis nær land. Undersøkelsene ble foretatt på to lokasjoner: på sjøis nær kystlinjen og på sjøisen 200 meter ut fra kysten. På hver lokasjon ble 4 trykksensorer fryst inn i isen. 3 av sensorene ble fryst inn på lik dybde i isen i en rosett, mens den fjerde sensoren ble fryst inn i en annen dybde for å undersøke trykkfordelingen gjennom isen. Tiltmeter ble satt på hver lokasjon for å måle inklinasjonen av isen. Maksimum trykk nær kystlinjen ble målt til 162 kPa. I tillegg ble det målt 4 trykk toppunkt over 90 kPa. Bøying av isen bidrog sterkt til trykkøkningene. Retningen for trykket var parallelt med kysten. 200 meter ut på isen ble maksimum trykk målt til 37.7 kPa. Hendelsen var relatert til en temperatur økning i overflaten i toppen av isen som ble forårsaket av overvann. Gjennom vinteren var trykket betydelig høyere nær kysten. Trykk på begge lokasjoner varierte med tidevannet. Isen ved kysten hadde høyest trykk ved lavvann, 200 meter ut fra kysten var trykket høyest ved høyvann.

Contents

Appendix

A MSc Thesis Template

Appendix

B Results of compression test

List of Figures

List of Tables

Chapter 1

Introduction

The arctic and arctic sea have become an area of growing activity due to the hydrocarbon resources and northern ship lanes. The increased activity requier infrastructure at the coast. Construction and developement of structures at the arctic shore are challenging due to the presence of sea ice during the winter. It is necessary to understand the behaviour of sea ice in order to operate in a safe and effective manner in the arctic.

The Van Mijenfjorden at Svea, Svalbard, has since 2002 been subjected for a range of internal stress measurments in sea ice. Moslet & Høyland (2003) and Caline & Barrault (2008) found a correlation between tidal cyclus and stress development. An investigation done by Teigen et al. (2005) showed that stress was induced thermally at increasing air temperature with no correlation with tide. Barrault & Høyland (2007) found no correlation of tide and stress, or that stress was induced thermally by air temperature. However it was believed that a large amount of snow coupled with spring tide generated stress when the ice got flooded and caused thermal expansion. The development of stress in the sea ice in Van Mijenfjorden is at this point still rising questions and requier further investigation to be fully understood.

The fieldwork in this thesis was performed in Van Mijenfjorden winter 2014. 8 stress sensors were installed at two different sites at the inner basin of the fjord. An inclinometer was registring inclination of the ice at each site. The hinge zone were mapped and profiled. In addition were density, salinity and thin sections of the ice measured and observed.

This paper summarize the conducted fieldwork and presents the result. The result are further analyzed and discussed. Data from February was not gathered due to malfunction of the stress sensor loggers.

Chapter 2

Theory

2.1 Definitions

Sea ice is the general term of frozen sea water which can be found as icebergs, broken off from ice shelfs, ice spray on structures, ships and natural objects, and the ice formed by freezing of seawater. The variety in appearance of sea ice makes it necessary to point out what the term "sea ice" is referred to. Here, the term sea ice is referred to the ice formed by freezing of sea water, either on the water surface, on top or below existing ice.

Sea ice differs from fresh water ice in that it is a multi-phase material consisting of fresh water, brine, gas and salts. The typical salinty in arctic waters is in the range between 31 and 34 ppt (parts per thousand). This is slightly lower than the normal salinty in the Atlantic ocean at 35 ppt. When a second material is dissolved in water, the effect is higher density and lower freezing point. Due to salt dissolvement the freezing point of sea water is about $-1,8\,°\mathrm{C}$, depending on the amount of salt. The salt is increasing the density of water from 1000 kg/m^3 to about 1025 kg/m^3.

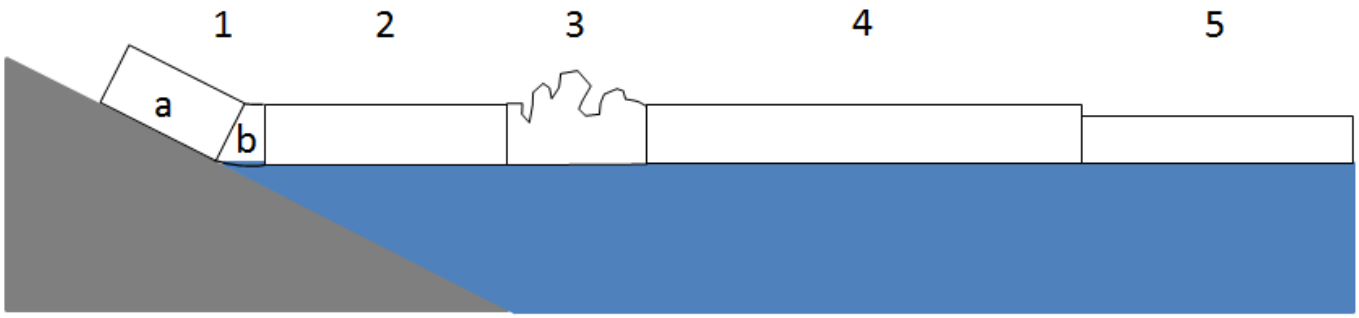

Figure 2.1: Classification of sea ice according to location. 1a) Ice foot, 1b) hinge zone, 2) landfast ice, 3) shear zone, 4) Pack ice or drift ice, 5) Marginal ice zone.

Classification of sea ice can be done according to location. The ice appearence varies as the location is moved from land to open water. The land and tide will affect the ice appearance because the tide is a moving system while land is fixed. According to this, sea ice is divided into five sub-groups based on location, as illustrated in figure 2.1.

1. Coastal ice, or shore ice, is affected by the presence of shore line. Coastal ice is further branched into ice foot (a), and hinge zone (b). The ice foot is fixed to the shore, while hinge zone is forming the transition to the free floating landfast ice. During tidal cycles, cracks are developed in the hinge zone as one end is fixed to shore while the other is moving vertically.

2. Landfast ice is connected to the shore through the hinge zone, but moves freely up and down during tide.

3. The boundary between landfast ice and drift ice is the shear zone. The shear zone is characterized by a high degree of deformation since the ice is fixed to the landfast ice but having interaction with drift ice.

4. Pack ice or drift ice that can move.

5. Marginal ice zone (MIZ) is defined as the transition between the drift ice and open water (Høyland 2013).

The investigation was done on two locations: at the landfast ice close to the hinge zone and on the landfast ice 200 meters further out. The two sites is referred to as Site 1 and Site 2 respectivly. At Site 2 the landfast ice is referred to as level ice in order to seperate the two sites. The main focus of the fieldwork was pressure induced in the landfast ice and the transition to the coastal ice through the hinge zone. Therefor will the shear zone, drift ice and marginal ice zone not be further commented or discussed in this thesis. Cracks is a widely term when speaking of sea ice. Cracks is a common feature of ice and appears wherever ice is existing. In this paper cracks are referred to as tidal cracks or thermal cracks.

2.2 Sea ice structure and growth

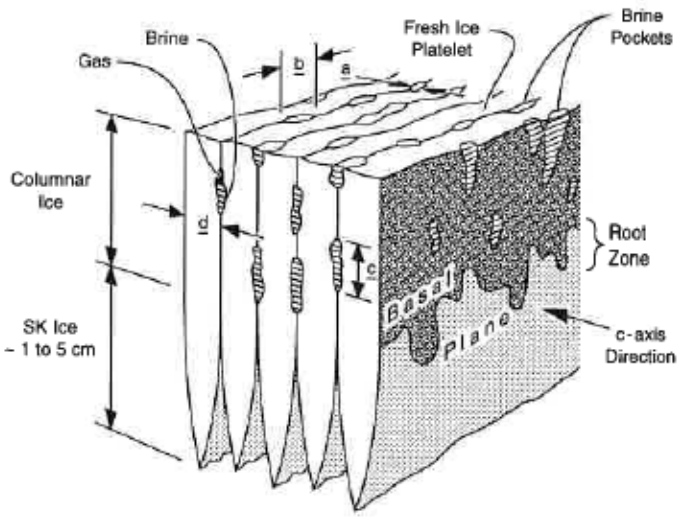

Figure 2.2: The grain structure for columnar ice. From Kovacs (1996)

Sea water freezes at approximately $-1,8\,°\mathrm{C}$, depending on the amount of salt. When the initial freezing starts, small crystals forms a layer of slush at the sea surface. The crystals will then coalesce to form a solid ice rind up to 5 cm thick. The next stage is the growth of solid ice. At this point the grains are about 1 mm in diameter and are frozen together randomly in an layer normally between 5 cm and 30 cm thick. This layer is known as granular ice. When the ice continue to grow at the bottom surface the crystal change appearance. The growth process is slowed down and the formation of larger crystals occur. These crystals are columnar in shape and are at first randomly orientated. The grain consists of thin plates of ice, platelets, which are bonded together with small pockets of brine trapped between. The plane of the platelets is called the basal plane. In this plane the crystals grow rapidly. Perpendicular to the basal plane is the c-axis, which has a significant slower growth rate. The basal plane and c-axis can be seen in figure 2.2. When the crystals has changed appearence to columnar ice, the crystals are randomly orientated. The crystals having a vertical basal plane will grow faster than the ones with vertical c-axis. There will be a competative growth where grains with vertical c-axis will be wedged out by the faster growing grains. At first are the crystals with vertical c-axis wedged out, then the one which is slightly tilted, then the one that is a bit more tilted, until all grains is having a horizontal c-axis and vertical basal plane. The layer of grains with vertical basal plane is dominant by large columnar ice crystals of size between 1-10 cm and sometimes larger. Typically in landfast first year ice the cover consists of a 30 cm layer of granualar ice, then a 50 cm layer of randomly orientated columnar ice, followed finally by preferentially orientated columnar ice (Sanderson 1988). When all crystals are columnar and the wedging out is finished, the c-axis of neighbouring grains can be horizontally different orientated, so called S-2 ice. If the grains is having a c-axis in the same direction, the term is S-3 ice. S-3 ice appear when the ice under influence of a steady current. If the current is steady to one direction, it will allign the grains in the direction of the current.

2.3 Mechanisms for generating stress in sea ice

Sea ice is a material which responds to external forces in the same manner as any other material. This means that sea ice expands when being rapidly heated, inducing thermal stress. Mechanical stress are induced from external forces acting on the ice sheet e.g. wind, current and tide.

Thermal stress

Thermal expansion and contraction is a materials respons to temperature changes and is according to Barrault & Høyland (2007) one of the major causes for stress induction in constrained sea ice. When the material is exposed to heating the kinetic energy in each molecule is increased. The spacing between them becomes larger when the molecules collides, resulting in a total volume expansion. If the volume is confined i.e. can expand with no interruption, the change in volume will not create any internal stress. If the volume is confined, an expansion will be impeded leading to a stress buildup. Thermal expansion occurs as a result of a change in temperature according to three basic principals:

1. A change in the air temperature at the surface. The temperature in the air will propagate through the ice cover acoording Fourier's law of heat conductivity. The propagation is dependent on the surface boundary layer and thermal diffusivity of the ice. This process can be impeded by an insulating layer of snow and wind disturbing the the thermal surface layer.

2. Transport mechanisms in the ice can be disturbed by the presence of air, rain or meltwater. Since sea is permeabel, it allows percolation into the ice which cause rapid temperature change.

3. Short-wave and long-wave radiation may be important factors of temperature change (Sanderson 1984).

To add a fourth principal it should be mentioned that flooding off the ice can change the temperature rapidly if the air temperature is low. The sea water hold a temperature of about $-1,8\,°\mathrm{C}$, and when flooding the ice, the upper layer will be exposed to a temperature increase causing thermal expansion.

An easy approach to describe thermal expansion is to look at it as a one dimensional beam, as in figure 2.3. In the first case the beam can expand freely with no interruptions. In the second case the beam is confined in length L.

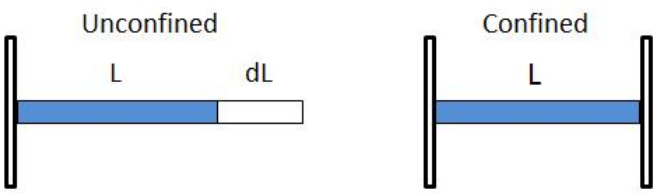

Figure 2.3: Unconfined beam to the left and confined beam at the right.

When the beam can freely expand, the change in length is as follows

$$dL = \alpha(t) * \Delta T \tag{2.1}$$

where α is the coeffient of thermal expansion and ΔT is change is temperature. Thermal strain, ϵ^t, can further be calculated by

$$\epsilon^t = \alpha(t) * \Delta T \tag{2.2}$$

The beam is now only subjected to thermal strain, hence the total strain equals to thermal strain

$$\epsilon^T = \epsilon^t \tag{2.3}$$

For the case with the confined beam, the elongation of the beam is restricted causing stress build up. The stress is basically calculated from Hooke's law which states

$$\sigma = E * \epsilon^T \tag{2.4}$$

where σ is stress, E is Young's Modulus and ϵ^T is the total strain. When substitute the total strain with the expression found in 1.2, the thermal stress can be found by

$$\sigma = E * \alpha(t)\Delta T \tag{2.5}$$

The coefficient of thermal expansion has at this point not any defined value for sea ice. Sea ice is a non stationary material so the coefficient is not constant. Further is sea ice a material with fresh water and brine as the biggest components which have different properties such as freezing temperature and thermal coeffisient. Adding the fact that the amount of salt is varying in the ice, a clear definition of the coefficient is hard to obtain (Ellingsen 2006).

Tide

Earlier measurments by Teigen et al. (2005) suggest a correlation between tidal cycles and stress development in landfast ice. The measurments show in general that the stresses were higher during low tide and decreasing during high tide. At high tide the ice is allowed more expansion and reduces the stress in the ice. At low tide the ice is more constrained and higher pressure is developed. The process is illustrated in figure 2.4.

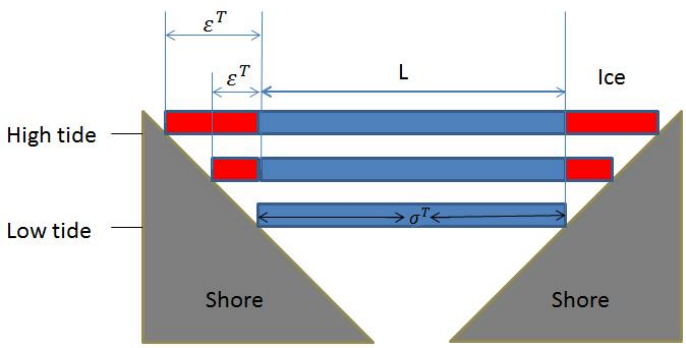

Figure 2.4: Stress development when the ice is more confined during low tide.

Teigen et al. (2005) performed stress measurments in the level ice in Sveasundet. A correlation between maximum stress and the direction of which the distance to the beach is longest was found. A model by Teigen et al. (2005) was suggested to explain the event. Consider a rectangular plane stress plate which is subjected to thermal stress. The minimum width of the plate is along the x-axis and the maximum width is along the y-axis. Suppose that the boundaries of the plate is partly confined. The partly confinement is of such character that the force needed to displace the plate increases with distance of displacement, like a spring being extended. Further is the plate experiencing a temperature increase ΔT. The temperature increase leads to a thermal expansion where the plate should, when unconfined, expand by

$$u_k^T = \epsilon_k^t \times L_k \tag{2.6}$$

where u_k^T is the expansion in direction k, ϵ_k^t is the thermal expansion in direction k and L_k is the width of the plate in direction k. When taken into account that the boundaries is partly the confined, the actual expansion will be limited to

$$0 < u_k < u_k^t \tag{2.7}$$

u_k is the actual expansion. The internal strain which generate stress will be the difference between the unconfined strain and the actual strain. The expression for the internal strain then becomes

$$\epsilon_k = \alpha \times \Delta T - u_k/L_k \tag{2.8}$$

where α is the one-dimensional coefficient of thermal expansion. The second term of the expression is depending on direction as the prescribed boundaries makes $u_x/L_x < u_y/L_y$, which again gives $\epsilon_x > \epsilon_y$. This means that larger internal strain will generate higher stresses. The topography around Braganzavågen and Sveabukta is mostly low inclinated beach coast where the ice is pushed onto during thermal expansion. The forces needed to push the ice onto the beach is higher when the distance to the beach is longest e.g. the thermal expansion is longest. The highest stress should occur in the direction where the distance to the shore is longest.

Cracks

Cracks is an important feature for developing and relaxing stress. Cracks can be developed due to high level of stress in the ice or reduce stress when the cracks gets closed. Sea water can leak into the cracks and freeze, which cause stress when the water expand during freezing.

Tidal cracks

The interaction between the hinge zone and the landfast ice creates tidal cracks. The driving force of a tidal crack is the tidal cycles. The crack is developed during the vertical movement of the ice during a tidal cycle as in figure 2.5. At high tide, the hinge zone is free floating on the water surface. When the water level drops during low tide, the motion of the hinge zone could be limited by grounding or freezing. When grounded, the coastal ice will not be able to follow the landfast ice further down as the water level continue to drop. Freezing occurs when the ice foot freezes and fastens to the shore.

As the water level drops at low tide, the fastend ice will be fixed to the shore and will not follow the downward motion of the landfast ice. Both freezing and grounding is causing stresses in the hinge zone leading to cracking as the ice yields.

Thermal cracks

Thermal crack is developed when the ice experience a rapid change in temperature. The crack is often created when the upper part of the ice contracts due to a change to colder temperature. Since the temperature is damped through the ice cover, the layers further down will not be that affected by the temperature change and will strive to maintain the structure. When the contraction of the top ice exceeds the tensile strength, the crack is opened. If the crack is penetrating the ice sheet, then it is called wet crack. If the propagation of the crack goes through the ice sheet, the term is wet crack (Barrault & Høyland 2007).

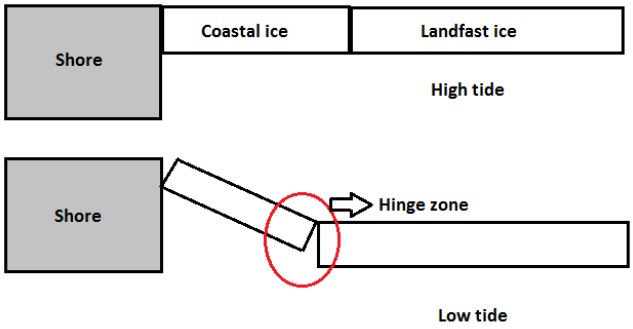

Figure 2.5: Generation of tidal crack due to the downward motion of landfast ice at low tide.

A hypothesis by Caline & Barrault (2008) suggests that stresses are developed when sea water fills tidal cracks during high tide. The water undergoes a rapid temperature decrease when coming in contact with cold air which leads to freezing and expantion. This leads to stress in the ice as the new ice expands in the confined volume of the crack. Barrault & Høyland (2007) suggest that the process may also occur in wet cracks. Sea water fills the crack which again freezes and expands. The newly formed ice is a weak point in the ice sheet, and the next crack is most likely to be developed in this weak point. The new crack is filled with water which freeze and expands, building up latteral stress in the ice. This process can be reapated numerous times.

Bending

It is well known that bending will generate tensile and compression stress in the material. As the ice is bend, tensile and compression will occur on opposite surfaces of the ice. The bending necessary can be provided by tide which generate vertical movement of the ice sheet. The ice sheet interaction with shallower water, shore and hinge zone can cause the ice to be restricted to follow the movement of the free floating ice. The transition to floating ice is experiencing an upward momentum generating compression on the top ice of the transition.

Dragforces

Mechanical stress is induced by external forces acting on the ice. Since sea ice is between air and water, it is subjected to forces over and under the ice sheet. Currents and tidal currents may create a dragforce on the bottom surface while wind create dragforces on the top surface. Wind generates stress as the friction between the moving air and ice affect the icesheet. The magnitude of the dragforce is a result of the area of the ice surface the wind fetches, wind velocity, air density and an air-ice drag coefficient. Teigen et al. (2005) suggest that wind in theory generate stresses in the same magnitude as the stresses measured in some events at a survey in Svea. However, it is not likely that wind is a major factor for stress generation that area. The main direction of the wind in Svea is east, whilst the fetch is generated west of the investigation site. Taken into account the geometry of the fjord which is long and narrow with a small opening, the wind direction needed for generation of stress is in a small range between 60° to 75° north. Currents is not believed to be of such magnitude that it would affect the stress level in the ice in Van Mijenfjorden (Caline & Barrault 2008).

2.4 Relaxation mechanisms

Thermal induced stress is a result of an increasing temperature. On the other hand, at a decreasing air temperature, quite the opposite is happening. The molecules will loose kinetic energy and move less around. The space needed for each molecule is less and the spacing between them will be reduced. The result is diminishing stress followed by a contraction of the ice. This is refered to as thermal relaxation (Barrault & Høyland 2007).

Brine pockets and brine channels may be an important process of relaxation. Brine pockets and brine channels is created as the brine migrate either downwards or upwards in the ice. The gaps is then open for the ice to expand into and relax the stress in the ice. However this effect seems to be seasoned dependent, when the ice-brine interaction is different early and late in the season. In the beginning of the season, the ice is considered a closed system. This means that there is low drainage of brine, and due to the fact that water has low compressibility, the ability to absorb stress is low. Later in the season have the salt mechanism been running and there is a high interconnection between the brine channels. The salt mechanisms drain the salt either to the bottom surface or the top surface of the ice and the gross salinity decreases with time. This leaves an open gap in the ice which can absorb the stress. The same relaxation is done by cracks. Cracks in the ice can reduce the stress significantly. The stress is absorbed by closure of the cracks as the ice expands (Barrault & Høyland 2007).

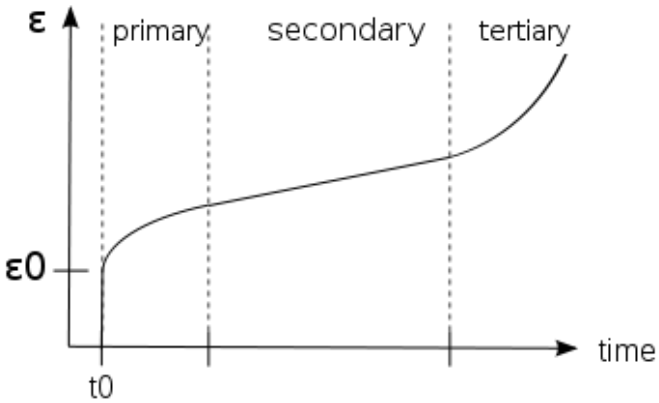

Figure 2.6: The stages of creep

Creep is the tendency of change in structure and shape permanently under the influence of stress. It occurs as a result of long term exposure to high level of stress that is below the yield point of the ice. The process can be shown in strain-time diagram as in figure 2.6. The figure show how creep undergoes three stages: primary, secondary and tertiary to failure. In the primary stage the material undergoes a strengthening. This is because the dislocations in the crystal structure glide in to a fixed order by the applied load. In the secondary stage the strain rate is near constant. This is due to a balance between strengthening and altering of the material. Relaxation occur when the stress diminish for the benefit of dislocations in the structure. In the tertiary the strengthening of the material ceases and the balance between altering and strengthening is disturbed. As the stress gets larger than the strengt, the ice yields. Moslet (2001) suggest that slow acting processes can affect the

ice and create internal stress in the ice cover over time. If the stress is applied at a slow rate, it can be relaxed in the secondary stage of creep.

2.5 Temperature distribution

The temperature distribution through the ice sheet is important to how the ice responds to changes in the air temperature. The temperature is damped through the ice until it reaches the temperature of the water in the ice-water interface. Normally through the winter this distribution is close to linear. In figure 2.7 the temperature gradient is illustrated through the ice cover. The damping effect through the ice is seen when the temperature rises from $T_{a,1}$ to $T_{a,2}$. The temperature change in the top surface is much larger than further down e.i. at the depth of the sensors at z_{sensor}. The linear decrease lasts until reaching the water temperatur (Sanderson 1988).

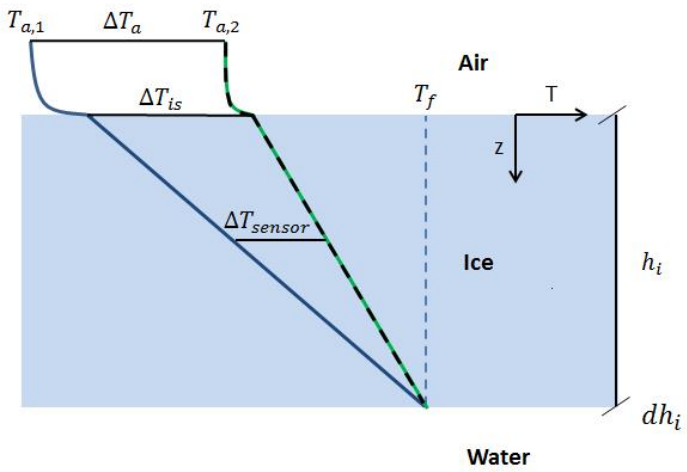

Figure 2.7: Temperature damping through the ice.

2.6 Salinity

Salinity in sea ice is due to entrapment of brine during freezing. The presence of brine and salt will affect the ice behavoir considering the different properites of salt, brine and pure ice. The amount of salt trapped in the ice is a dependent of the grow rate of the ice, which is directly related to air temperature. An example is shown in figure 2.8.

Granular ice at the top has higher salinity, typically beween 8 - 12 ppt, because of the rapid freezing of the water. As the ice thickness grow, the grow rate slows down and salt is more effectivily expelled from the ice as is freeze. Brine occurs then in small pockets trapped between the platelets of the columnar ice. The brine is here in a stable equilibrium with the surrounding ice. The salinity of the brine must be of such concentration that it can coexist with the surrounding ice. At $-1,8\,°\mathrm{C}$ the salinity is 35 ppt, but as the temperature drops, pure water crystallises out of the brine, leaving a more concentrated brine which can coexist with ice at the new colder temperature. Over time the

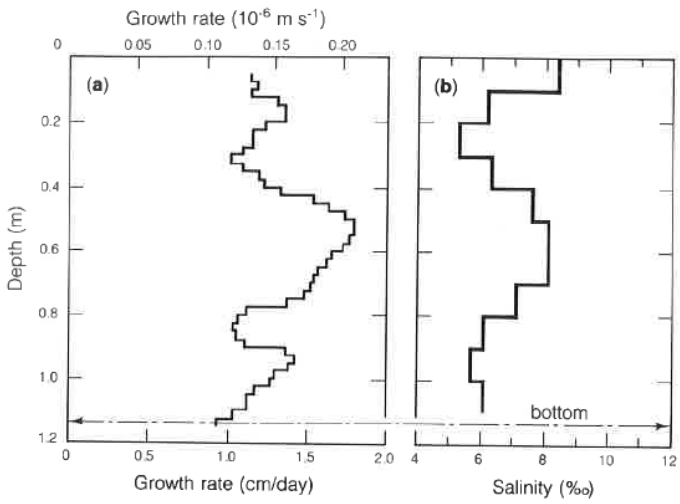

Figure 2.8: Growth rate (a) of ice in relation with salinity (b) in Eclipse Sound, NWT (Nakawo & Sinha 1984).

brine migrate either to the top suface or bottom surcafe of the ice, where it is expelled. The migration downwards is due to gravity and temperature gradient, while the upward migration is due to a reversed temperature gradient when the temperatuer is warmer on the top surface than the bottom surface.

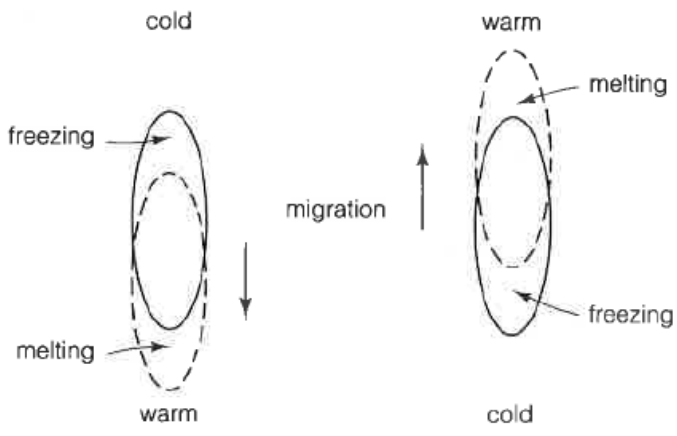

Figure 2.9: Schematic diagram of migration of brine pockets along vertical temperature gradient in winter (a) and spring (b) (Sanderson 1988)

When the ice is having a temperature gradient throught the ice cover, then it is more energetically favourable to melt the warm end of the brinepocket and refreeze the cold end. The result is a migration of brine towards the warm end. During winter the temperature gradient is going from the cold air to the warm water, and the brine migrates downwards. The pockets will become larger and longer as they migrate since the sourroundings is getting warmer (Sanderson 1988).

2.7 Snow

Snow is an important parameter affecting the sea ice behaviour. Snow is in general having a high content of entrapped air, which reduce the thermal conductivity significantly. When the ice is covered with a layer of snow, the snow will provide a layer of insulation to the ice, and the temperature at the ice-snow interface will be higher than in the snow-air boundary. The cold air temperature will be damped through the snow cover and thermal effects in the ice will be reduced (Bergdahl 1977). Barrault & Høyland (2007) suggest a correlation between large amount of snow resulting in reduced boyancy and generation of stress in landfast ice. Large amount of snow affect the ice bouancy. As the weigth of snow overgoes the bouancy of the ice, the ice sink below the waterline which floods the ice. The flooding may cause rapid expansion of the layer of the ice because of thermal expansion. In addition will the brine experience a reversed pressure gradient from the bottom of the ice sheet to the top. As the brine migrate upwards, the open cavities in the top layer gets filled and thereby reduce the relaxation of stress.

2.8 Major and minor principal stress and principal direction

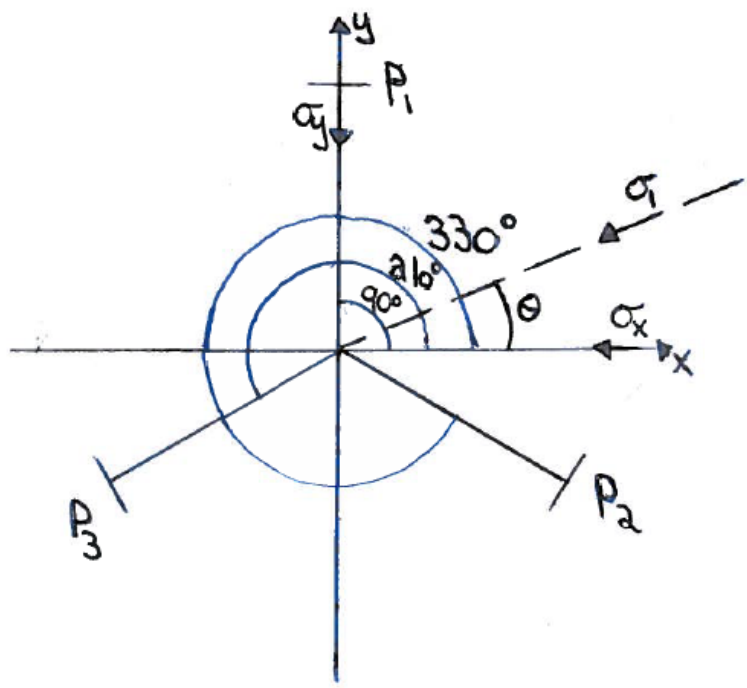

Figure 2.10: Major and minor principal stress found by measuring stress at three points: P_1, P_2 and P_3.

The major and minor principal stress is the extreme values for normal stresses in a material. The orientation of the principal stress is the principal direction. Prinsenberg et al. (1997) derived a expression for the principal stress and the direction. Basically the expression takes into account three points that measure stress in different directions, as in figure 2.10. The three points is named P_1, P_2 and P_3. The coordinate stresses can be then calculated from the three points by

$$\sigma_x = -\frac{1}{3}P_1 + \frac{2}{3}P_2 + \frac{2}{3}P_3 \tag{2.9}$$

$$\sigma_y = P_1 \tag{2.10}$$

$$\tau_{xy} = -\frac{1}{\sqrt{3}}P_2 + \frac{1}{\sqrt{3}}P_2 \tag{2.11}$$

Further can the principal stress be calculated from the measured stress exclusively

$$\sigma_{1,3} = \frac{1}{3}(P_1 + P_2 + P_3) \pm \sqrt{\frac{4}{9}(P_1^2 + P_2^2 + P_3^2 - P_1P_3 - P_1P_2 - P_2P_3)} \tag{2.12}$$

The direction of the major principal direction is given, counterclock wise from σ_x, by

$$\tan 2\theta = \frac{2\tau_{xy}}{\sigma_x - \sigma_y} \tag{2.13}$$

where θ is the angel from σ_x.

Chapter 3

Site and experimental set up

3.1 Site

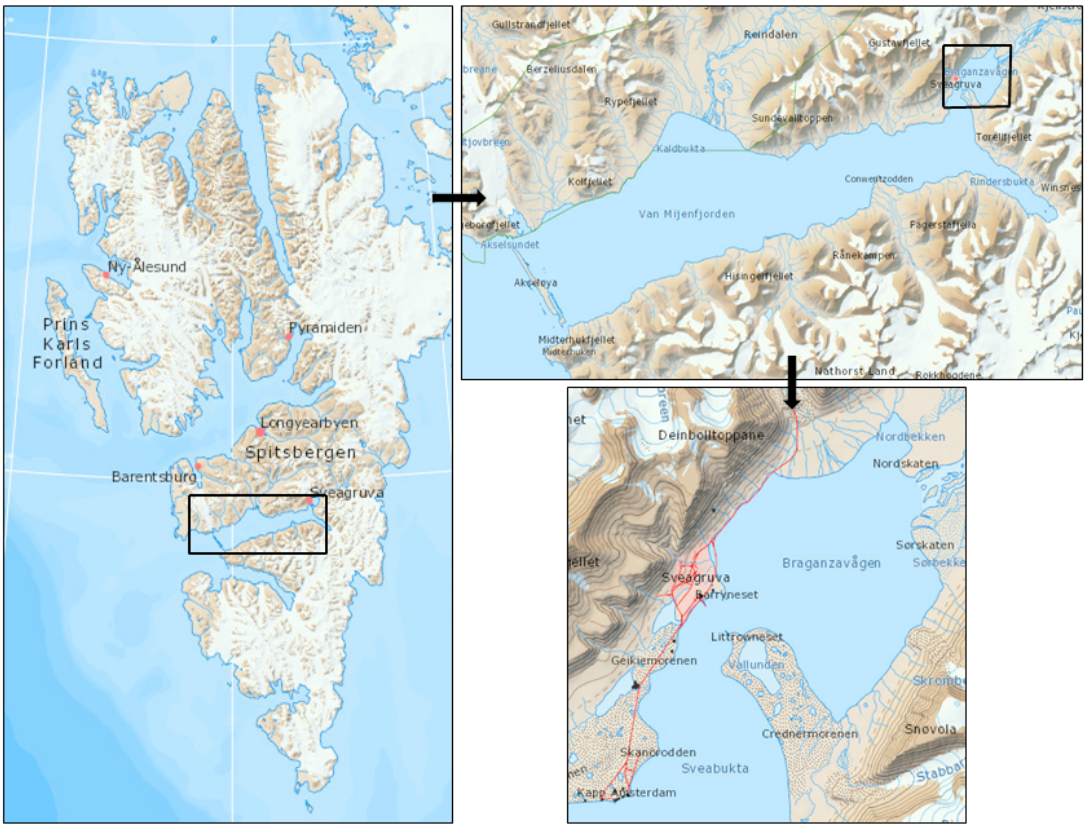

Figure 3.1: Spitsbergen and the Van Mijenfjorden area. Braganzavågen and Sveabukta in the bottom right picture. Map is provided by The norwegian institute of polar research (The Norwegian Institute of polar research 2014).

The fieldwork was conducted in the strait to the inner basin of Van Mijenfjorden at Spitsbergen, Svalbard. The area of investigation is shown shown in 3.1. Svalbard is an archipelago in the north-western Barents Sea. During winter 2014, sea ice covered the northern and eastern waters around Svalbard. To the west and south the sea was open water, except for fast ice in the inner fjords. Van Mijenfjorden is located at latitude 77 °48′, and a main bearing of 70 ° to north. The fjord is cutting in from west, and closed in the east by a glacier and mountain area of Heer Land. An island in the fjord inlet, Akselæya, is creating a natural boundary which ensures an undisturbed and stabile icegrowth in the fjord. Since 2002 a range of measurments of internal ice stress have been conducted in Van Mijenfjorden.
The inner basin of Van Mijenfjorden, called Braganzavågen, is connected to the fjord through a strait between Braganzavågen and Sveabukta. The basin is typically 5 km wide with an average depth of 30 meter. The two investigated sites was located in the strait, called Sveasundet. As seen in figure 3.1 the strait is confined by land in nearly every direction. A small headland, Barryneset, is reaching into Sveasundet from north. Site 1 was directly at the seaside of the last tidalcrack at Barryneset and Site 2 was on the landfast ice in the strait 200 meters south of Barryneset which is shown in figure 3.2. Similar investigations have been performed in the hinge zone by Caline & Barrault (2008), Gabrielsen et al. (2008) and Østerås et al. (2011). Results from previous stress measurments in level ice is represented in Moslet & Høyland (2003), Teigen et al. (2005) and Barrault & Høyland (2007). The thin section procedure was performed in Coldlab 2 at UNIS, Longyearbyen.

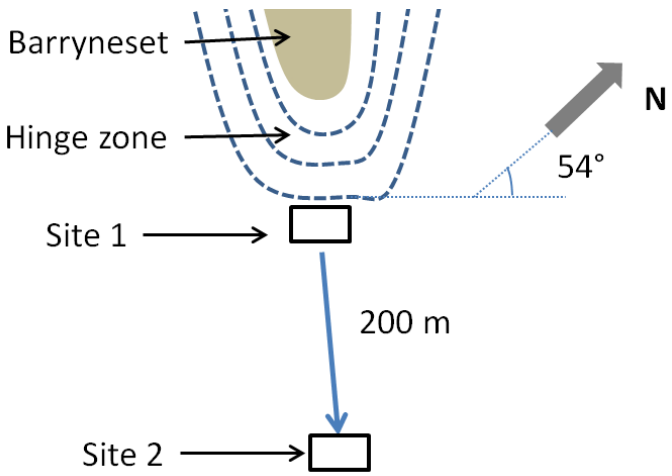

Figure 3.2: The experimental sites. Site 1 was located in the hinge zone at Barryneset. Site 2 was 200 meters further south in Sveasundet.

All transportation of equipment and personell to and from Svea was done by snowmobiles provided by UNIS. The transport from Longyearbyen to Svea took approximently 2 hours depending on conditions and amount of equipement. Lodging and food in Svea was arranged by Store Norske Grubekompani Spitsbergen.

3.2 Instrumentation

Pressure sensors

The internal ice stress was recorded using a Geokon Model 4800 Earth pressure cell. The pressure cell was connected to a Geokon RS-232 Datalogger with four channels. The datalogger will be referred to as datalogger 1 and datalogger 2 for the two sites respectivly. Each channel were connected to one pressure cell. Stress registred in the pressure cells are converted to an eletrical signal transmitted to the logger memory. The 320K standard memory in the logger provides storage for 10666 data arrays. Each array consits of the pressure reading, datalogger ID-string, a timestamp consisting of the year, month, date, hour, minute and second when the reading was taken. In addition the logger reads internal logger temperature, battery voltage, transducer temperature and array number. The arrays were collected through a RS-232 Communication Cable (DB-9F to 10-pin Bendix Male), to a laptop. Data was monitored and collected using LogView, a Geokon proprietary Graphic User Interface (GUI) software application. LogView was used to set the logging intervall which was in the range of 10s to 300s. The datalogger was powered by two 1.5 V alkaline batteries.

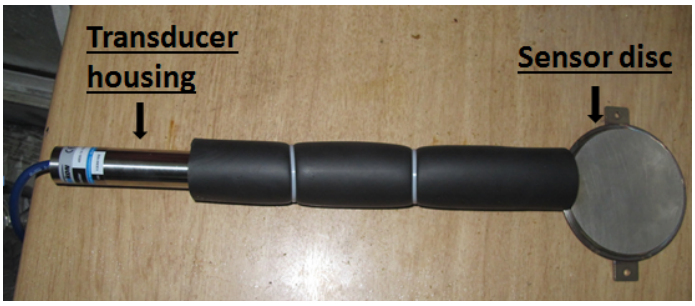

Figure 3.3: Geokon Model 4800 Earth pressure cell.

Earth pressure cells are constructed from two stainless steel plates welded together around the periphery. The narrow space left between the plates is completely filled with de-aired hydraulic oil. The pressure induced in the oil by external pressure is converted to an eletric signal by a vibrating wire in the transducer housing. The eletrical signal is then transmitted through a signal cable to the readout location. Located in the transducer housing is a thermistor for measurment of temperature at the cell location. Temperature is internally calculated as the resistance in the thermistor varies when the temperature change (Geokon 2011). The thermistor housing is 20 cm over the pressure cell, so the temperature measured was not taken at exactly the location of the pressure cell. The sensor is shown in figure 3.3. For the two investigated sites there were used three sensor models. The models are described in table 3.1.

The calibration of the sensors were done according to a supplied calibration sheet from Geokon. The calibration was done in LogView by inserting the given calibration factor G and a thermal factor K. The thermal factor provides a correction for the temperature effect on the transducer alone. The calibration factor is converting the digits, which is the unit for measurment and reduction of data from the pressure cell, into pressure readout Geokon (2011). Resolution was 0.025 % of given sensor

Sensor	Model	Heigth	Disc diameter	Thickness	Pressure range
Site 1	4800-1X-700 kPa	45 cm	10 cm	6 mm	0 - 700 kPa
Site 2, sensor 1 and 2	4800-1-350 kPa	58.5 cm	23 cm	6 mm	0 - 350 kPa
Site 2, sensor 3 and 4	4800-1-2 MPa	58.5 cm	23 cm	6 mm	0 - 2 MPa

Table 3.1: Sensor dimensions

Sensor	Model	Min. Accuracy	Max. Resolution
Site 1	4800-1X-700 kPa	3.5 kPa	0.175 kPa
Site 2, sensor 1 and 2	4800-1-350 kPa	1.75 kPa	0.0875 kPa
Site 2, sensor 3 and 4	4800-1-2 MPa	10 kPa	0.5 kPa

Table 3.2: Sensor accuracy and resolution

reading, and the accuracy was 0.5% for given sensor reading (Geokon 2011). For resolution and accuracy, the extreme values is given in table 3.2.

Tiltmeter

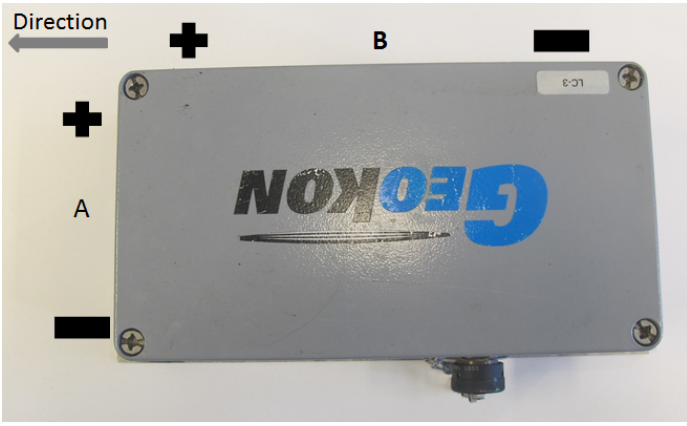

Figure 3.4: Tiltmeter. The direction is defined were channel B is positive.

To measure the inclination of the ice a Geokon LC-3 Datalogger Model 8003D2, with biaxial MEMS tiltmeters, was installed. They were installed at Site 1 and Site 2, and will respectively be referred to as tiltmeter 1 and tiltmeter 2. The logger was powered by three 1.5 V alkaline batteries. Using the biaxial MEMS tiltmeter the logger provided data for two uniaxial directions. The directions is referred to as A and B, after the marking on the tiltmeter, as shown in figure 3.4. The internal memory of 512K provides storage for 21000 data arrays. Each array consits of MEMS tiltmeter reading, datalogger ID string, a timestamp of year, month, date, hour, minute and second. In addition is battery voltage, datalogger temperature and array number recorded. Temperature is measured as the resistance in the thermistor change when temperature change. The datalogger is configured and monitored using LogView. Data were downloaded through an USB interface to a laptop. Options for logging intervall

was in the range from 5 to 86400 seconds. Calibration of the tiltmeters was done in LogView with calibration directions given from Geokon Inc (Geokon 2011). When delivered from Geokon, the tiltmeters were zero set at 0 °. The range of measurment is ±15 ° in both directions, but the tiltmeter can be adjusted to preferred orentation using an adjustment key. This was however not necessary in this case. The accuracy of the tiltmeters was 0.01% of sensor reading, and resolution was 38.15μV. For the thermistor the overall accuracy was 1.0% of sensor reading (Geokon 2011).

Ice core sampling

Ice cores were extracted using a collective auger produced by Cocax. The auger is cylindrical and hollow with a lenght of 100 cm and an inner radius of 7,1 cm. The auger is designed to collect ice when it is driven down in the ice. A set of blades in the opening of the covax ensures proper cutting of the ice. The covax was mounted to a Hitachi DH 36DAL, a 36 volt battery powered drill. To measure ice thickness and freeboard two-inch augers were used. The augers are produced by Covax in stainless steel with a lenght of 100 cm and thikness of 5 cm (2 inches). At the top and bottom of each auger there is a connector where another auger can be connected to extend the reach. A blade bit is at the end of the last auger to cut the ice.

Thin sections

Thin sections were prepared with a Leitz mircotome shaving instrument. The microtome is a mechanical milling instrument having a jacking range between 1μm to 40μm. The shaveblade is rigid above the ice sample while the platform, where the ice is placed, is jacked upwards at each shave. The platform have furrows in the surface which is connected to a KNF No22AN.8 vacuum pump. The vacuum pump ensures fastening of the sample. When the sample is shaven down to a thickness of 1 mm, the sample is illuminated from underneath and observed through a polarized glas which is fixed above the sample.

Salinity and density

The salinity was measured with a Metler Toledeo SevenGo Conductivity meter SG7. Calibration was done by using a predefined solution which were provided by Metler Toledo. The accuracy is ±0.5% of the measured value. Density was calculated from height and weight which were measured with a ruler and a KernKB weight. The accuracy of the ruler was ± 3mm and the accuracy of the weight was ± 0.1 g.

3.3 Method

Stress sensors

The stress measurment setup consisted of four stress sensors at each site. Three of the sensors were installed in a rosette with 120 °N spacing between each sensor and the distance from sensors center

to rosette center were 15 cm. A fourth sensor was placed 1 meter from the rosette. The sensors were numbered counterclock wise from the referance sensor: sensor 1. Figure 3.5 show the schematic setup of the sensors. The set up at Site 2 was identical as figure 3.5 without the hinge zone.

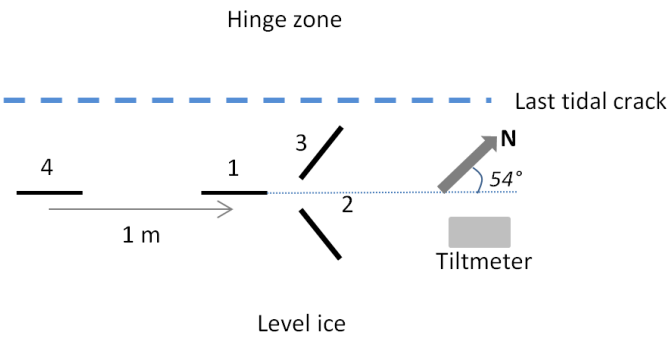

Figure 3.5: Schematic view of the sensors and tiltmeter.

Installation of the sensors was done by removing snow and placing a pre made wooden stencil on the ice surface. The stencil was a template for the rosette placing. Sensor 1 at Site 1 was used to orientate the stencil, as the sensor was orientated parallel with the last tidal crack south of Barryneset. The bearing of the tidal crack and sensor 1, was 54 °N. A GPS with a compass function was used to obtain the same orientation for the rosette at Site 2. When the stencil was placed, slits were cut in the ice with a chainsaw. As the stencil was removed, the slots was cut to desired depth of the sensor. Sensor 4 was installed at a different depth to observe the variation of stress distribution in the ice cover. The depth of the sensors is shown in table 3.3. The width of the slots was between 1 and 2 cm. It is adviced to have the slots as narrow as possible to get a proper confinement of the ice surrounding the sensor. At insertion the sensors were jerked up and down to avoid airpockets to be trapped between the sensor and the sourrounding ice. After installation the slots were backfilled with salt water. The salinity of the added water was based on the salintiy in the top most ice where the sensors were installed. During the first two weeks of january overwater flooded the ice leaving the datalogger under 20 cm of seawater. Seawater leaked into the logger causing it to malfunction.

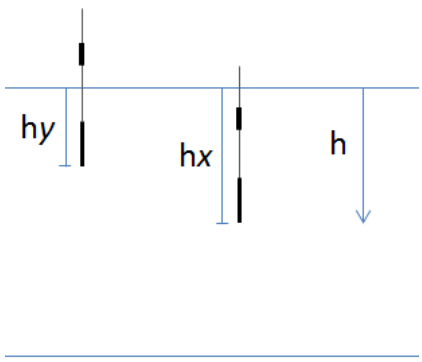

Figure 3.6: Schematic display of the sensors at the different depths hy and hx.

Sensor	Depth [cm]	Date	New depth [cm]	New date
Site 1, Sensor 1	hy = 12	30.01 - 12.03	hy = 20	12.03 - 09.05
Site 1, Sensor 2	hy = 12	30.01 - 12.03	hy = 20	12.03 - 09.05
Site 1, Sensor 3	hy = 12	30.01 - 12.03	hy = 20	12.03 - 09.05
Site 1, Sensor 4	hx = 18	30.01 - 12.03	hx = 25	12.03 - 09.05
Site 2, Sensor 1	31	30.01 - 12.03	hx = 20	30.03 - 09.05
Site 2, Sensor 2	31	30.01 - 12.03	hx = 20	30.03 - 09.05
Site 2, Sensor 3	31	30.01 - 12.03	hx = 20	30.03 - 09.05
Site 2, Sensor 4	31	30.01 - 12.03	hy = 12.5	30.03 - 09.05

Table 3.3: Sensor depth and duration.

Once bitten twice shy the logger was placed on a pallet. During the campaign the sensors on both sites were moved. At Site 1 they were moved due to a detection of a tidal crack on the seaside of the sensors. The sensors were moved to the seaside of the crack the 12th of March. The sensors at Site 2 were extracted based on a suspicion of malfunction. This was proven not to be correct, and they were reinstalled at the same place the 30th of March.

The extraction was done by cutting a 5 cm thick frame around each sensor. The frame was cut to the depth of the sensor. When the frame was cut, the ice covering the sensors were removed by a gently use of pry bar and sledgehammer.

Tiltmeter

To get the inclination of the ice, a tiltmeter was placed at each site. The tiltmeter was firstly put directly on the ice, but was later left on two pallets to elevate it from the ice surface. A pallet has a big ground coverage, which will follow the inclination of the ice. To ensure that the tiltmeters was firmly placed, the pallet was frozen to the ice using slush, and the tiltmeter was nailed to the pallet. This turned out to work good, until extraction where the pallet was frozen solid to the ice. The direction of the tiltmeters were changed during the fieldwork, the directions and dates is listed in 3.4. The direction is defined as the positive direction of B to north, see figure 3.4.

	Site 1	Site 2
Direction/date	130° / 30.01 - 19.02	310° / 30.01 - 19.02
Direction/date	135° / 19.02 - 12.03	90° / 19.02 - 12.03
Direction/date	234° / 12.03 - 10.05	54° / 12.03 - 10.05

Table 3.4: Tiltmeters: direction and date.

Ice core sampling for salinity, density and thin sections

When extracting ice samples the hollow auger was attached to a battery powered drill. As the hollow auger was drilled through the whole ice thickness, the drill was detached and the sample was carefully

slid onto a plastic half pipe. The samples were cut into 10 cm and 7 cm pieces, put in boxes and transported to UNIS for laboritory testing. The temperature was sub zero during the transportation. Ice samples were retrieved from Site 1 and Site 2 at every visit. The samples were retrieved in close proximity of the sites, but at different locations to avoid disturbance of the stress measurments.

Hinge zone profile

The hinge zone was profiled from the coastal bluff at Barryneset, through the hinge zone until the ice was level. To make sure that all ice- interaction at shore were covered, the measurments continued outwards until the landfast ice had a constant thickness. Firstly a meterband was stretched from a fixed stick at the bluff to the landfast ice. Then holes were drilled through the ice each 2 meters from the bluff. When entering the landfast ice, the distance was increased to 3 meters. At each hole there was taken measurments of ice thickness, freeboard and snow depth. The place where the ice was grounding was found during drilling. A stick with a fixed ruler and a nail, for finding the bottom ice surface, was used to measure ice thickness.

Thin section

The thin section were performed in Coldlab 2 at UNIS, at temperature -20°C. The thin section procedure demanded a preparation of the ice before using the microtome. Firstly it was cut out a 2 cm horizontal piece from the sample. The piece was placed on a 8 cm x 8 cm glas plate which was 2 mm thick. The ice was then frozen to a glasplate using water at freezing point. The free end of the ice was shaven until it was completely flat, and a second glas plate was fastend to the free end. When the second plate was fastend, the sample was cut in two between the glasplates. The first glasplate were put away, while the second was placed in the microtome. When the plate was fixed with vacuum, the ice was shaven down to 1mm. When the sufficient thiness was obtained, the sample was placed over a lightsource. The sample was then observed though polarized glas where the grains appeared in different colors for the different orientations of the c-axis.

Salinity and density

The salinity measurment were done after the sample had been put in boxes and left inside for melting. Once melted the salinity was measured with a conductivity meter. To make sure the sensor was clean between each sample, it was rinsed in two boxes with destilled water. The density of each sample was found by

$$\rho = \frac{m}{V} \tag{3.1}$$

where ρ is density, m is mass and V is volume.

Ice thickness, freeboard and snowdepth

The ice thickness was found by drilling a hole through the ice and measure the ice with a stick with a fixed ruler and a nail to find the bottom surface of the ice. Freeboard was measured from the ice

top surface to the water surface using a ruler. Snowdepth was found using a ruler.

An overview of the campaign

Trip #	Date	Work	Comment
1	30.01 - 01.02	Installation of instruments Ice core retrieved for salinity	
2	19.02 - 20.01	Site 1 : Datalogger taken back to UNIS Site 2 : Datalogger taken back to UNIS Site 1: Sensor 4 taken back to UNIS Tiltmeter 1: new direction Tiltmeter 2: new direction Site 1: ice core for salinity and density Site 2: ice core for salinity and density Hinge zone profile	30 cm of overwater Flooding of instruments Datalogger 1 malfunctioned 02.02
	01.01	Site 1: new datalogger installed by David Wrangborg	
3	12.03 - 14.03	Site 1: Relocation of sensors, reinstallation of sensor 4 Site 2: Retrieval of all stress sensors Tiltmeter 1: new direction Tiltmeter 2: new direction Site 1: ice core for salinity and density Site 2: ice core for salinity and density Hinge zone profile Site 1: ice core for thin section	
4	30.03 - 03.04	Site 2: reinstall all sensors Site 1: ice core for salinity and density Site 2: ice core for salinity and density Hinge zone profile Site 1: ice core for thin section Site 1: ice core for compression test Site 2: ice core for compression test	
5	24.04 - 25.04	Site 1: ice core for salinity and density Site 2: ice core for salinity and density Hinge zone profile Site 1: ice core for thin section	
6	09.05 - 10.05	Site 1: Retrieval of all instruments Site 2: retrival of all instruments Site 1: ice core for salinity and density Site 2: ice core for salinity and density Hinge zone profile Site 1: ice core for thin section	End of campaign

Chapter 4

Results

4.1 Stress measurments

The stress data was collected at every visit throughout the campaign, from installation the 30th of January to retrivial the 10th of May. During the campaign there was some problems regarding the sensors and the logger. For Site 1 there is no recordings from the 2nd of February to the 1st of March. This was due to the flooding of the ice. Seawater leaked into the logger causing it to malfunction. A new logger was installed the 1st of March. From the 12th to the 13th of March the sensors were taken out and reinstalled at the seaside of the last crack at Barryneset. The 23rd of March the battery in the logger ran out. New battery were replaced the next visit at the 30th of March. The results from the 30th of January to the 2nd of February will be neglected since the period of time is short compared to the period of measurments later in the season.

For Site 2 the logger was brought back to UNIS the 19th of february for testing after the flooding. The sensors were extracted the 12th of March for testing based on a suspicion of misreadings from sensor 3 and 4. After testing and reconfiguration both logger and sensors were working properly and reinstalled the 30th of March. As Site 1, the batteries ran out the 23rd of March and replaced 30th of March. The 10th of May were the sensors extracted, marking the end of the fieldwork season.

All x-axis in the graphs in this section is counting hours from the 1st of January 2014, 00:00. When referred to the x-axis ,it is denoted hx, where x is hours from start e.g. 2200 hours from 1st of January 2014, 00:00, is denoted h2200.

Site 1

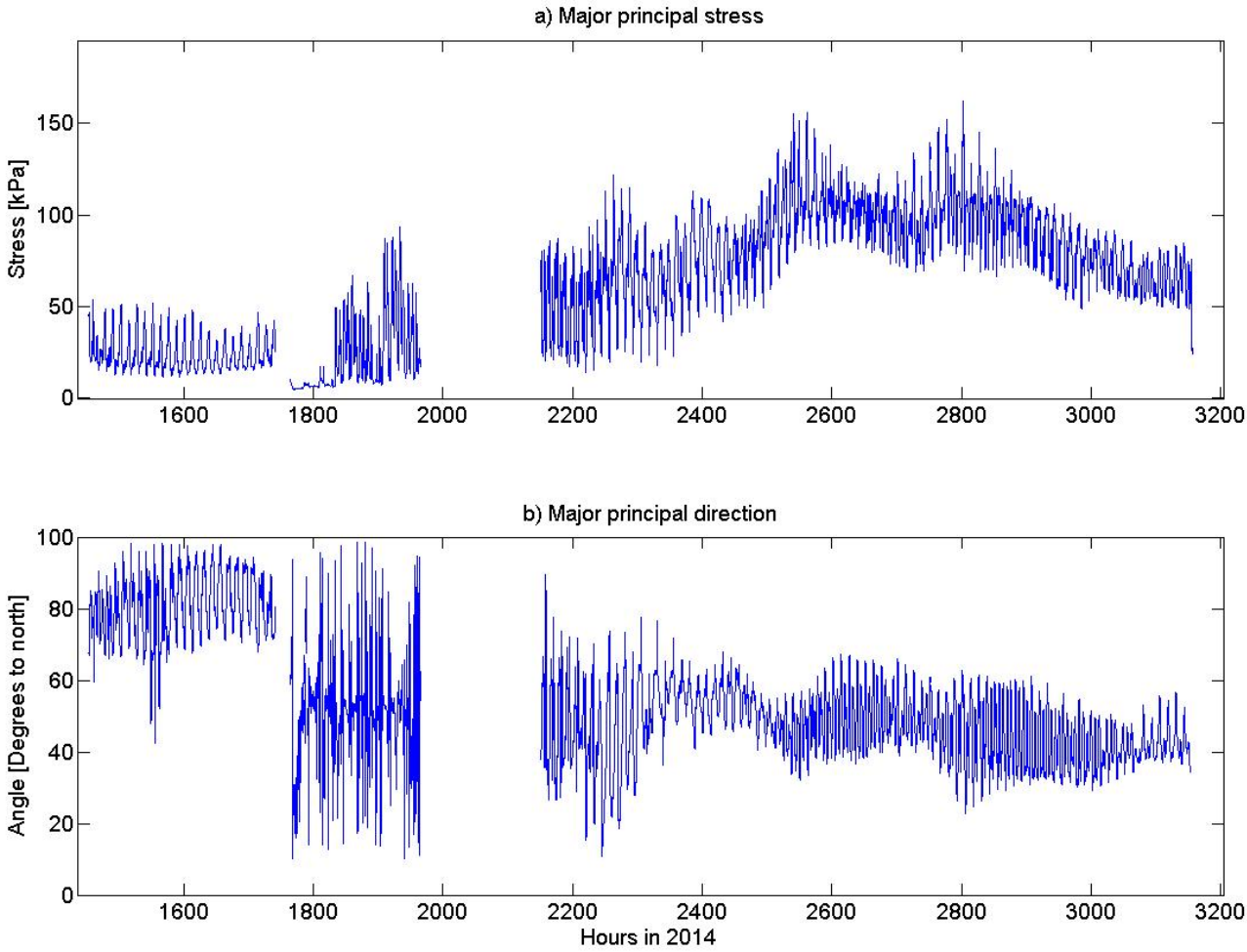

Figure 4.1: Site 1: Principal stress (a) and direction (b) from the 1st of March to the 10th of May.

Figure 4.1 show the major principal axis (a) and the major principal direction (b) at Site 1 from the 1st of March to the 10th of May. In the first period, from h1450 to h1750, the sensors were located on the landside of the last tidal crack. It can be seen that this period stands out regarding pressure and direction. The stress is between 15 - 50 kPa and the direction is between 65° and 100° to north.

The second period is from h1750 to h1950. The period end when the batteries in the logger ran out. The lowest stress of 5 kPa was recorded the days following the reinstalling of the sensors at h1750, but this was due to the freeze-in of the sensors. The stress recordings is then having a leap to a local maximum value of 93.1 kPa at h1930.

The third period lasted from h2150 to h3150. During this period there were four siginificant

maximum stress events. A global maximum where registred to 162 kPa at h2800. The four other main events have peak of 93.1 kPa at h1930, 121 kPa at h2260, 113 kPa at h2390 and 155 kPa at h2560. All the main events occures during an general increase in stress from h2150 to h3150. The direction of the events is between 45° and 50° to north, ergo parallell to the south tip of Barryneset where the sensors were installed.

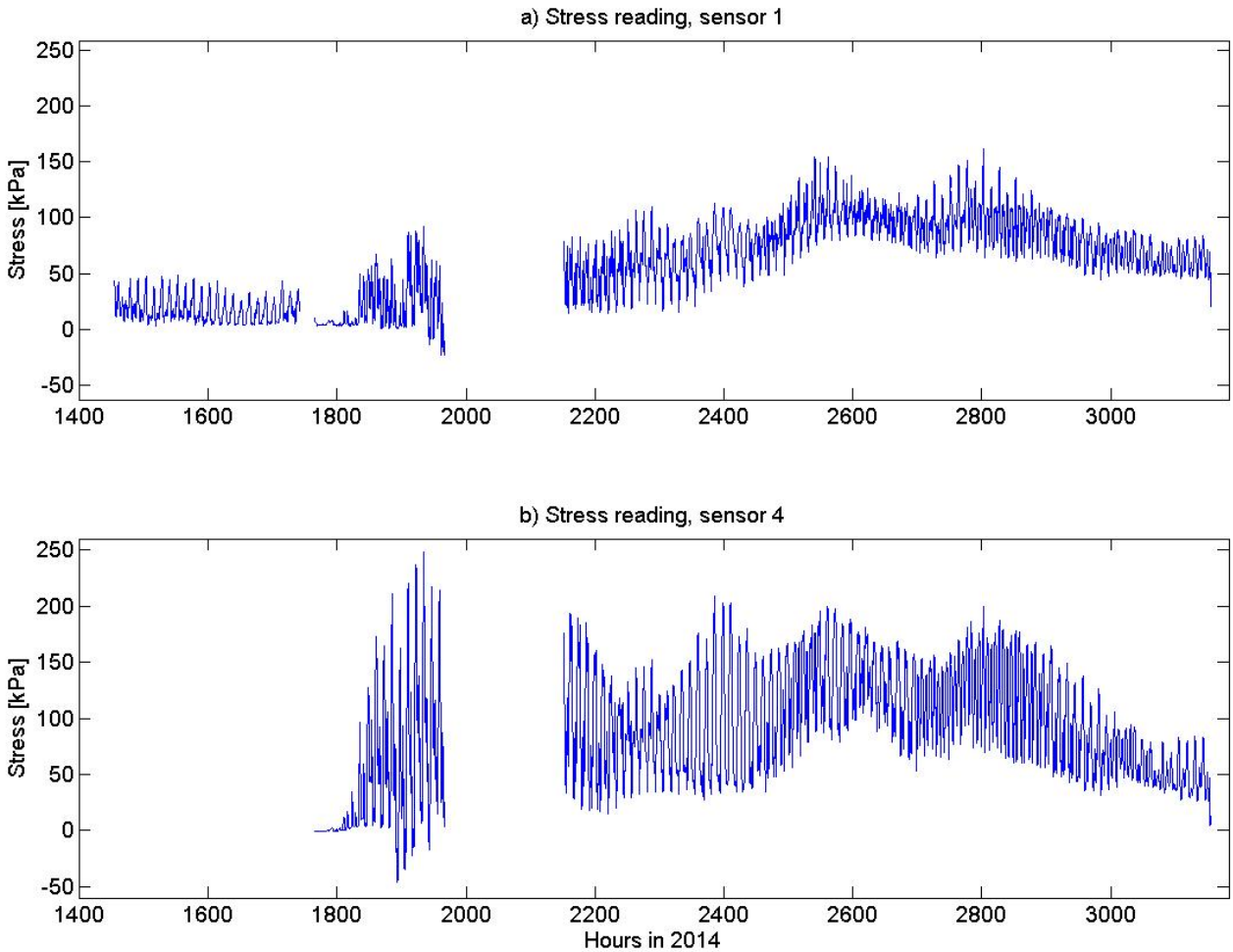

Figure 4.2: Site 1: stress measured in sensor 1 (a) and sensor 4 (b) from the 1st of March to the 10th of May.

Figure 4.2a) is measurments from sensor 1 and figure 4.2b) is measurments from sensor 4. The first period, from h1450 to h1750, is sensor reading from the first location of Site 1. At this point sensor 1 was installed at 12 cm depth but sensor 4 was not installed.

The second period is from h1750 to h1950. At h1750 was the sensors moved and reinstalled deeper in the ice. Sensor 1 was installed at 20 cm depth and sensor 4 was installed at 25 cm depth. In

the second period the stress is significantly higher in sensor 4 than sensor 1. Sensor 4 show a global maximum of 248 kPa at h1950.

The third and last period is from h2150 to h3150. In this period is the stress at sensor 1 showing four stress peaks. The peaks occur at h2300, h2400, h2550 and h2800. The event at h2800 was the global maximum for sensor 1, measuring 162 kPa. Sensor 4 is having the same development as sensor 1, and the four peaks in sensor 1 can be recognized in sensor 4, but with higher values. The stress was in general periodically fluctuating during the season and the recorded values was higher in sensor 4 than sensor 1.

Key data

4 significant principal stress events at were registred at Site 1 during the campaign. Each event is investigated more thorouglhy and the results are shown in table 4.1a to 4.1e. The events are listed chronologically after occurence as event #1 to event #5.

Table 4.1: Key parameters for principal stress main events at Site 1.

(a) Event#1 at h1930.

σ_{max}	93.1 kPa
dσ/dt	3.1 kPa/h
Build-up time	27 h 30 min
Relaxation time	8 h 30 min

(b) Event#2 at h2260.

σ_{max}	121 kPa
dσ/dt	3.5 kPa/h
Build-up time	30 h
Relaxation time	67 h 50 min

(c) Event#3 at h2390.

σ_{max}	113 kPa
dσ/dt	2.1 kPa/h
Build-up time	41 h
Relaxation time	45 h

(d) Event#4 at h2560.

σ_{max}	155 kPa
dσ/dt	1.6 kPa/h
Build-up time	67 h 30 min
Relaxation time	100 h

(e) Event#5 at h2800.

σ_{max}	162 kPa
dσ/dt	1.5 kPa/h
Build-up time	60 h 35 min
Relaxation time	194 h

Site 2

The principal stress and principal direction at Site 2 is illustrated in two separte figures; figure 4.3 and figure 4.4. The separation of the season is because the stress were not registred from the 19th of February to the 30th of March.

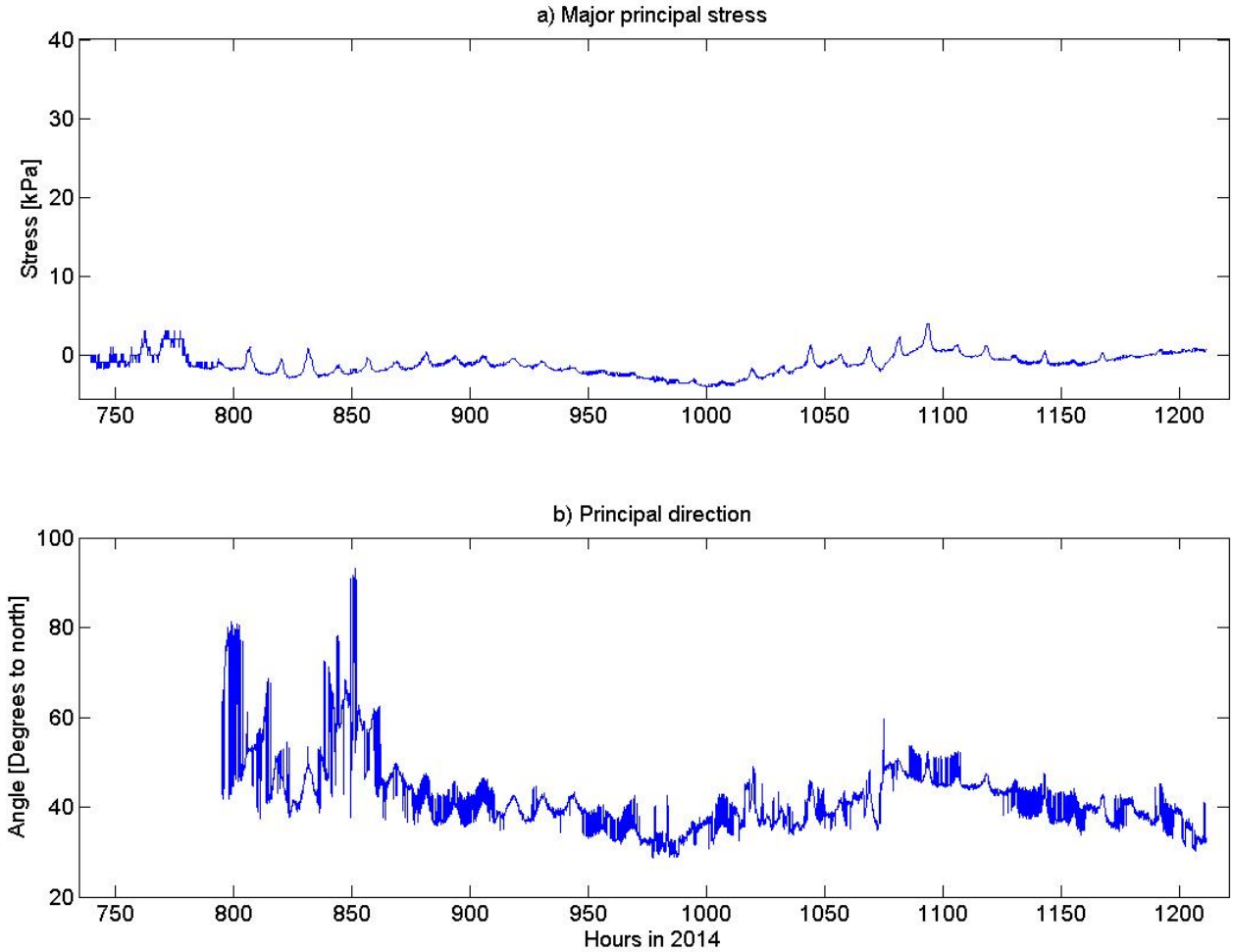

Figure 4.3: Site 2: Principal stress (a) and direction (b) from the 30th of January to the 19th of February.

Figure 4.3 show the major principal stress (a) and direction (b) from the 30th of January to the 19th of February. The stress was locally fluctuating with a defined maximum peak and a less defined minimum at each cycle. The maximum stress occurd as a single event at h1090. The maximum stress was 10.2 kPa and the direction was 50° north. The stress measurments did not show any significant events and the stress was generally low in this period.

The direction of the stress in this period is between 30° and 55° except for two events. The first event is at h800 where the direction is 80° north. The second event is h850 where the direction is 90° north. It can be seen in the figure that there is no data of direction from h730 to h790. This is because of the low resolution of Sensor 3. Due to the low resolution of the sensor, the output reading was either 0 or 1 kPa. The calculation of the direction was then highly variable and gave not a trustworthy result.

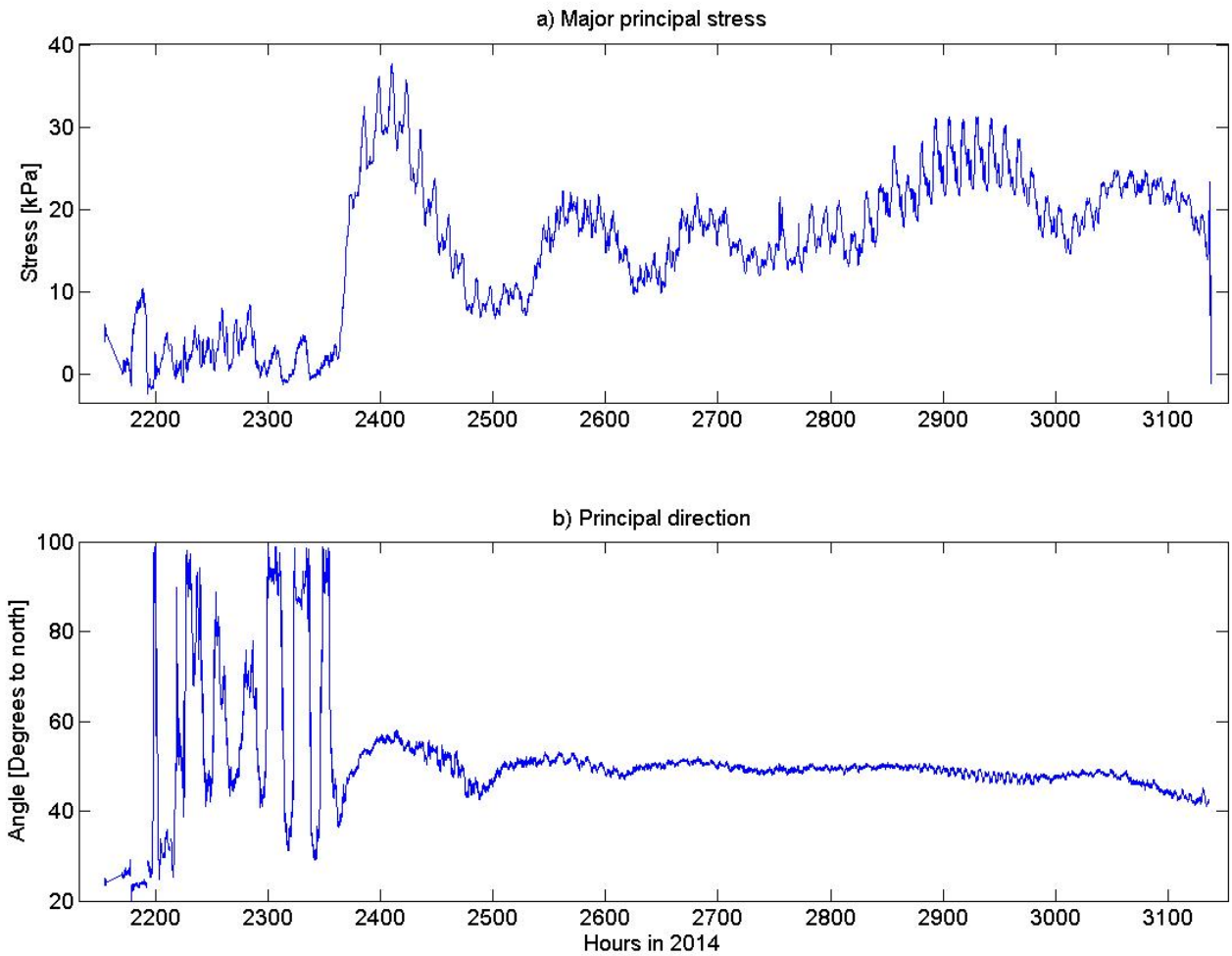

Figure 4.4: Site 2: Principal stress (a) and direction (b). 30th of March to 10th of May.

The second period is from the 30th of March to the 10th of May. The results is presented in figure 4.4. The stress is having regular local flucutations and irregular global flucutations. The local fluctuations are following the global trend in the way that the local variations are bigger when the global trend reach a peak. From h2150 the stress is between 0 and 10kpa until h2350. At this point the stress increase to the maximum value of 38 kPa at h2400. The stress is from this point in general

higher, with four distinct peaks having local maximums between 20 and 32 kPa. Towards h3150 the stress is slightly decreasing.

All the local maximum stresses develop in a time where principle direction is stable between 45° and 55° to north. The direction of the global maximum stress is shifted 4° further east than the four subsequent maximums. The direction is fluctuating between 25° and 100° from h2200 to h2370.

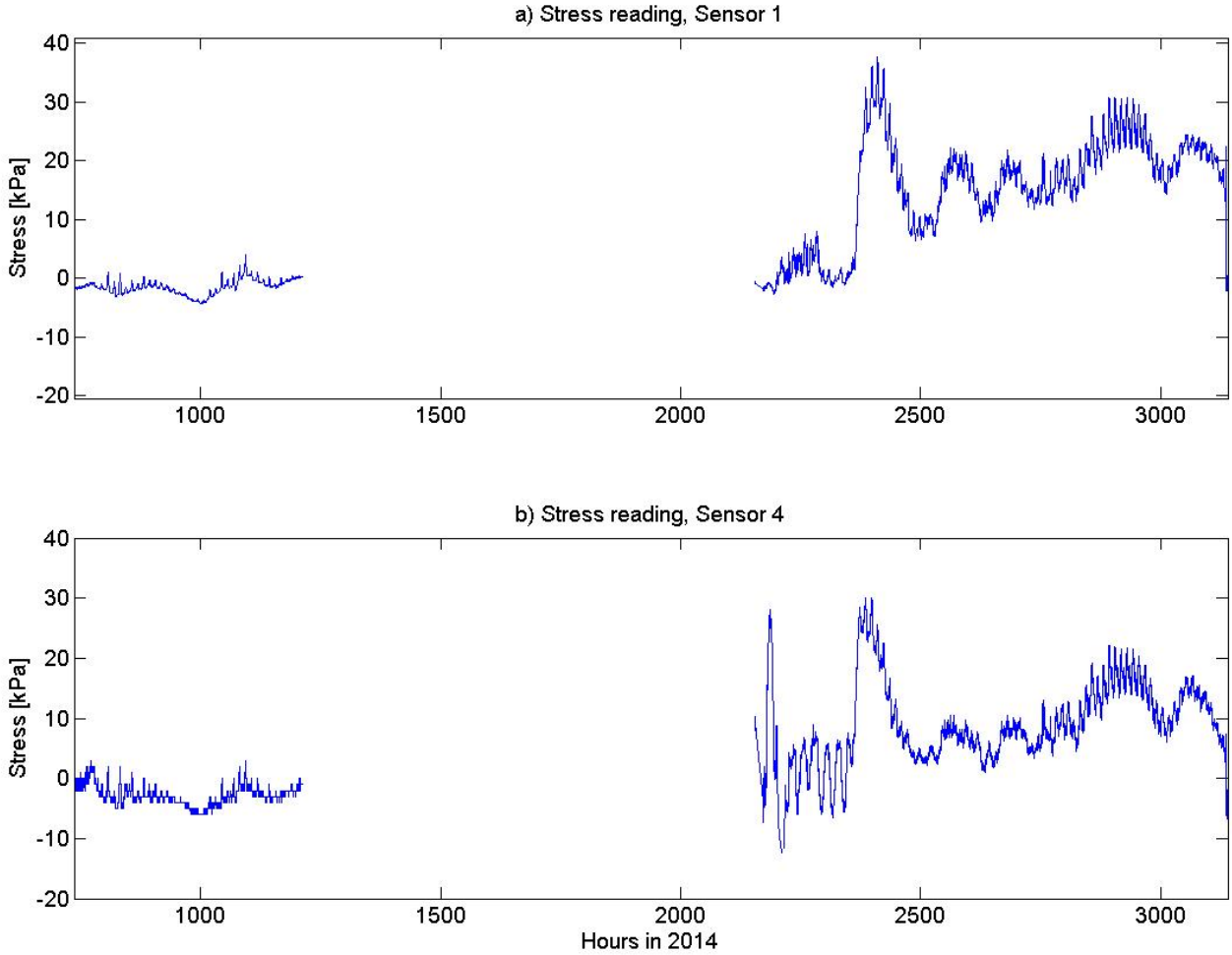

Figure 4.5: Site 2: stress measured in sensor 1 (a) and sensor 4 (b) from the 30st of January to the 10th of May.

Figure 4.5 show the stress in sensor 1 (a) and sensor 4(b) from the 30th of January to the 10th of May. The sensors were initially installed at the same depth at 20 cm. It can be seen in 4.5 from h750 to h1300 that sensor 1 and sensor 4 show more or less same stress reading. Sensor 4 is indistinct and show more variation, but that is because of the low accuracy of the sensor at that time. When the sensors were reinstalled at h2150 the accuracy of sensor 4 was similar to sensor 1, but the sensors were installed at different depths. Sensor 1 was installed at 20 cm, and sensor 4 was installed at 12.5 cm. After reinstallation the two sensors show different stress development. The stress in sensor 4 is from h2150 fluctuating until it reach maximum of 30 kpa at h2400. Sensor 1 is in this period having a more stable development until the maximum stress of 37 kpa at h2400. From this point and to h3150 the stress in the two sensors are showing the same trend, but sensor 4 have lower stress and less global

fluctuation. Both sensors have local maximums at h2560, h2680, h2930 and h3060.

Key data

5 significant principal stress events were registred at Site 2 during the campaign. Each event is investigated more thorouglhy and the results are shown in table 4.2a to 4.2e. The events are listed chronological after occurence as event #1 to event #5.

Table 4.2: Key parameters for principal stress main events at Site 2.

(a) Event#1 at h2400.

σ_{max}	37.7 kPa
dσ/dt	1.3 kPa/h
Build-up time	47 h 35 min
Relaxation time	79 h 5 min

(b) Event#2 at h2560.

σ_{max}	22.3 kPa
dσ/dt	0.45 kPa/h
Build-up time	32 h 45 min
Relaxation time	62 h 55 min

(c) Event#3 at h2680.

σ_{max}	22kPa
dσ/dt	0.38 kPa/h
Build-up time	31 h 30 min
Relaxation time	56 h 5 min

(d) Event#4 at h2930.

σ_{max}	31.3 kPa
dσ/dt	0.17 kPa/h
Build-up time	105 h
Relaxation time	83 h

(e) Event#5 at h3060.

σ_{max}	24.8 kPa
dσ/dt	0.19 kPa/h
Build-up time	53 h
Relaxation time	69 h 10 min

4.2 Inclination

Site 1

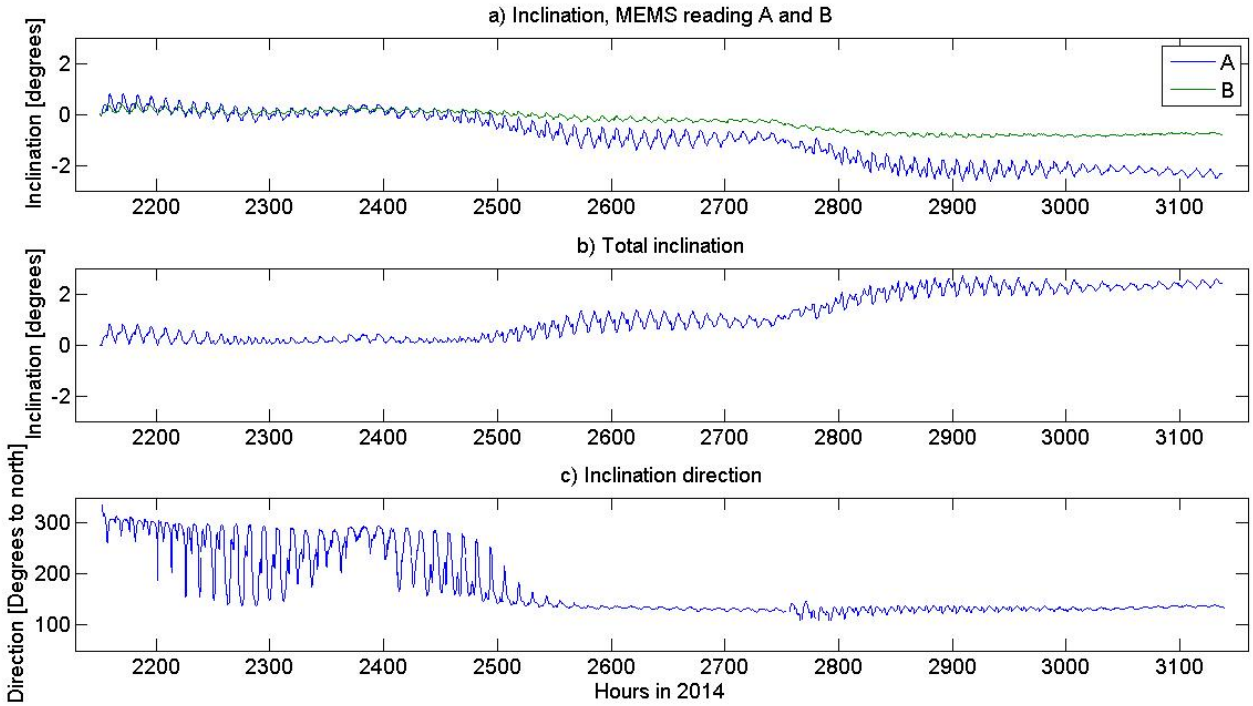

Figure 4.6: Site 1: a) MEMS reading of direction A and direction B, b) Total inclination, c) Direction of inclination.

The tilt at Site 1 from the 30th of March to the 10th of May is shown in figure 4.6a) - c). Figure 4.6b) show a local periodic fluctuation of the total inclination. The global trend of the total tilt is dominated by two step increases where the first last from h2500 to h2600 and the second last from h2750 to h2900, and reaching a maximum tilt of 2.7° at h2930. The direction in figure 4.6c) show that the direction fluctuates between 140° and 290° from h2150 to h2500. Further is the direction changed to 110° - 140° at h2500, which is perpindicular to the hinge zone. The change in direction occurs simultaneous as the first step increase in the total tilt.

Site 2

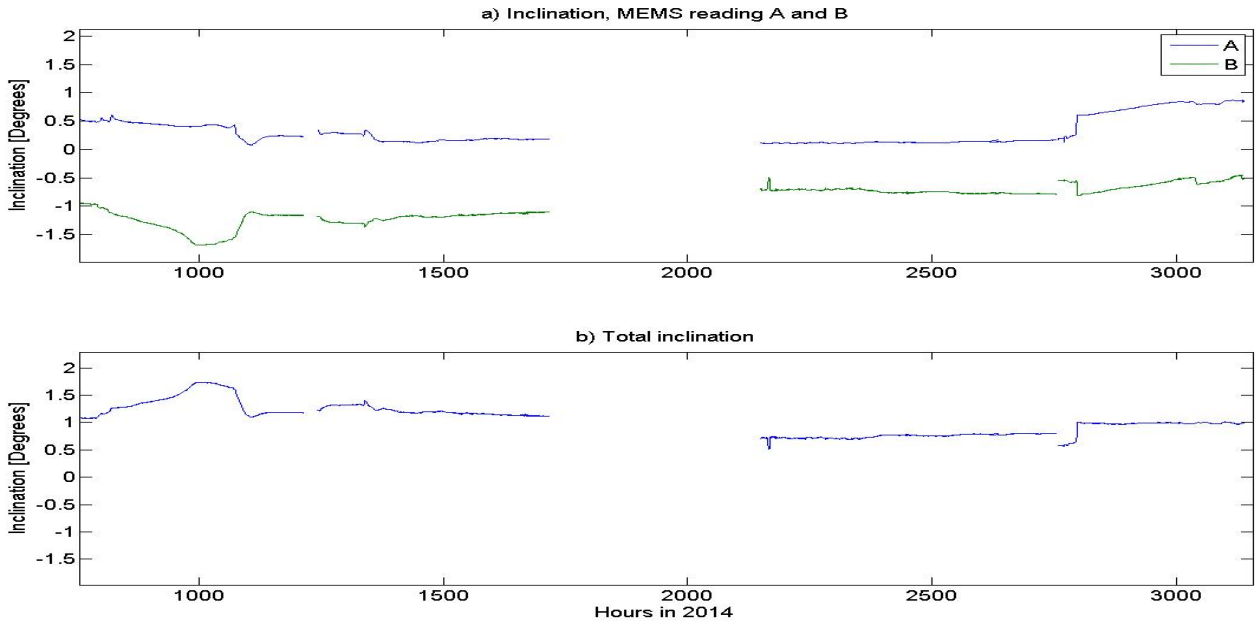

Figure 4.7: Site 2: a) MEMS reading of direction A and direction B, b) Total inclination, c) Direction of inclination.

Figure 4.7 presents the results from the tiltmeter at Site 2. The period between h1700 and h2150 is not having any inclination readings. This is because the tiltmeter was not set to record during the visit to the site at h1700. The error occurd as a consequence of incapability of the operator. The total inclination in figure 4.7b) is increasing with 0.7° from h750 to h1000. From h1070 to h1100 the total inclination decrease with 0.5°. The change in inclination at h2800 is because the tiltmeter was moved.

4.3 Hinge zone profile

During the fieldwork profiles of the hinge zone were made on high tide and low tide. Every profile showed more or less the same result, therefore will only one be presented. The profiles, shown in figure 4.8, was taken during high tide and low tide the 31th of March.

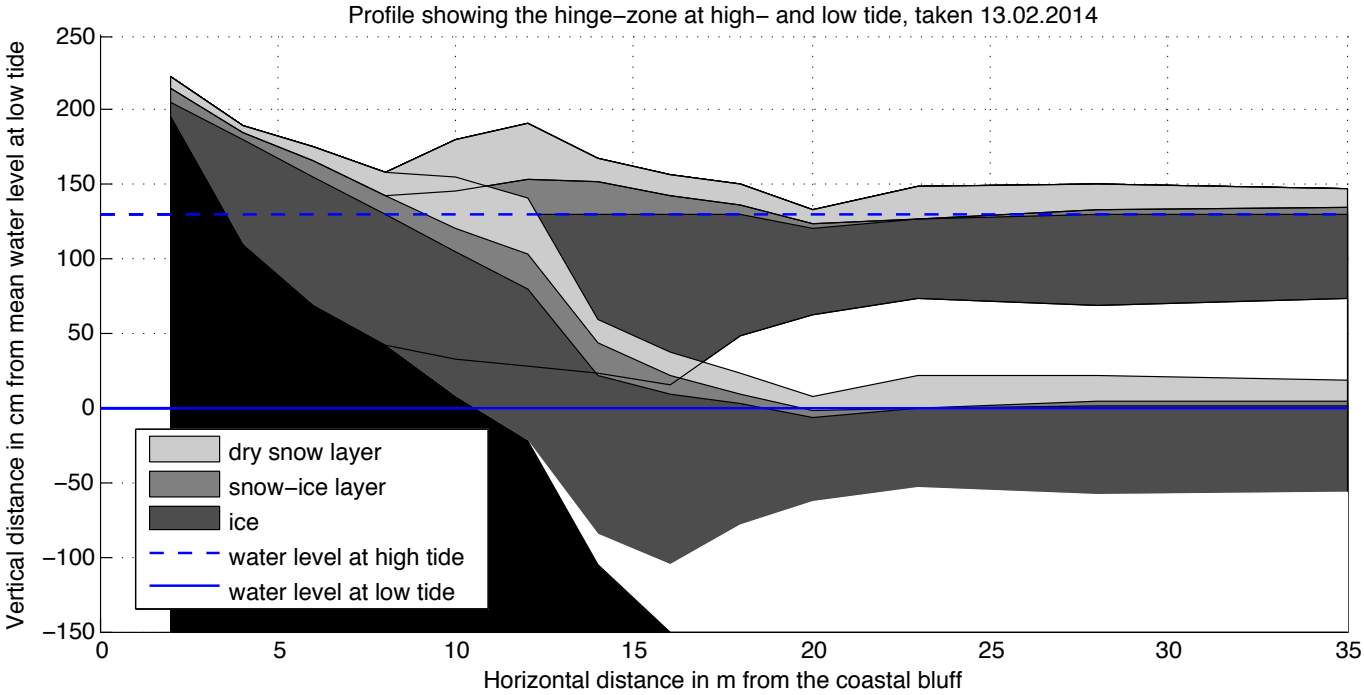

Figure 4.8: Profile of the hunge zone during high and low tide.

The profile show the ice relation to shore and vertical movement of the hinge zone at high tide and low tide. The darkest area is the shore profile, until 8 meters where it could no longer be detected. The upper profile is taken during high tide, and the bottom profile is taken during low tide. The difference between high and low tide was assumed to be 1.3 meters. The profiles startes from the coastal bluff in the very beginning of the landfast ice and moving out to level ice. The figure starts 2 meters from the coastal bluff. The snow and ice layer in the first two meters were diffuse due to the small thickness. The figure shows that ice is grounded until 8 meters at high tide. At low tide the ice is grounded up to 12 meters. From 8 meters to 23 meters there is a reorganisation of the hinge zone at high tide relative to low tide. After 23 meters the ice is rigid with no reorganisation, and the profiles is similar on both high tide and low tide.

Thin section

Thin section sequence was performed on samples taken the 12th of March from Site 1. The samples taken the 24th of April and the 10th of May were unfortunately melted before the thin section was done. The samples were retrieved after a period with overwater on the ice in february. From each samples there was taken horizontal and vertical thin section. In total was 6 samples observed. The results is shown figure 4.9 to figure 4.14. The series of figures start from the ice top surface to the ice

bottom surface. The figures of vertical sections is orientated with the upper layer of the ice at the top.

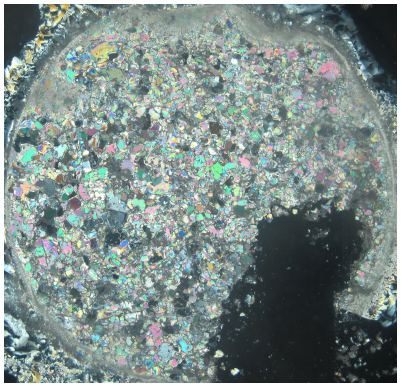

(a) Horizontal cut. 4.5 - 5.5cm.

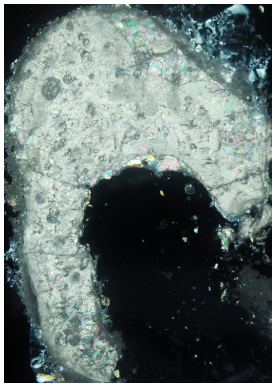

(b) Vertical cut. 0 - 4.5cm

Figure 4.9: Horizontal and vertical thin section from Site 1 at the 12th of March. Depth: 0 - 5.5cm.

Figure 4.9 is the thin sections taken from the top layer of the ice. The horizontal cut in 4.9a show a small grain size which is randomly orientated. The grains are granular. No airbubbles or brine pockets/channels is detected. The vertical section in 4.9b show airbubbles and brinepockets trapped in the ice. The sample got broken during shaving because of high porosity. The sample was not shaven down to the preferred thickness and the result show little of the structure of the ice.

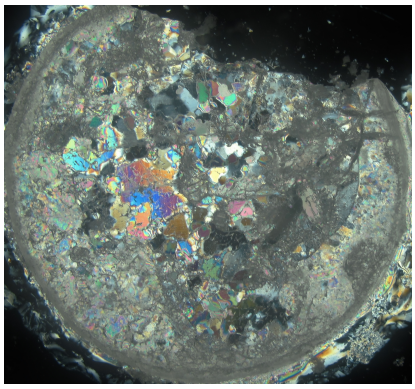

(a) Horizontal cut. 12 - 14cm.

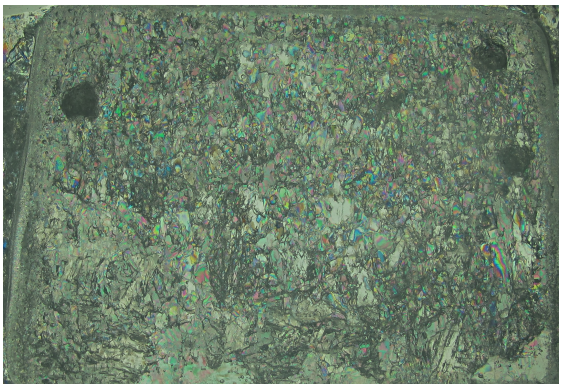

(b) Vertical cut. 5.5 - 12 cm

Figure 4.10: Horizontal and vertical thin section from Site 1 at the 12th of March. Depth: 5.5 - 14cm.

The high porosity of the sample in figure 4.10 restricted the thinness of the ice. However can it be seen larger grain size at this depth and some impurities in the horizontal cut. This is most likely brine pockets. From the vertical section in figure 4.9b the grains in 4.10b has come into a more defined structure. This is probably due to the thickness of the last sample. In figure 4.10b can it be seen three black areas which is brinepockets. The grains is in general bigger at the bottom of figure fig:ts5.5b, but it is still granular ice.

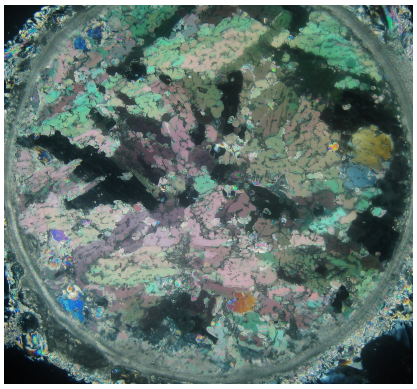

(a) Horizontal cut. 22 - 24cm.

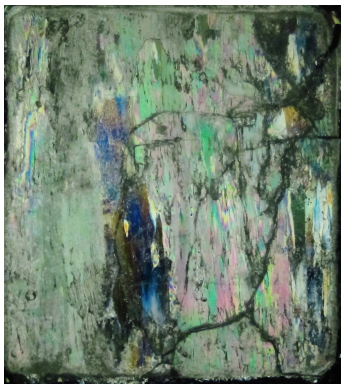

(b) Vertical cut. 14 - 22 cm

Figure 4.11: Horizontal and vertical thin section from Site 1 at the 12th of March. Depth: 14 - 24cm.

The grains in 4.11b is still growing compared with the last sample. It could be observed some black dots which could be brine channels. The grains in the vertical cut is at this point more columnar with basal plane in the vertical direction. In the top right corner is a black area which seems to be brine migration to a brine pocket. The sample cracked during shawing which explains the dark lines in figure 4.11b

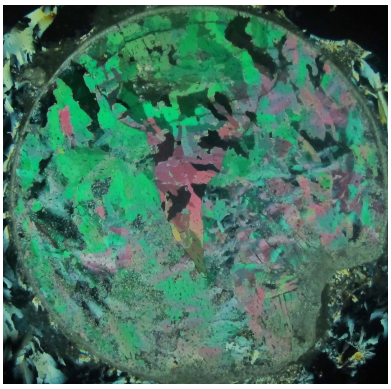

(a) Horizontal cut. 31 - 33.5cm.

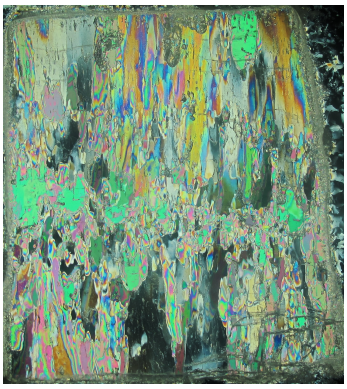

(b) Vertical cut. 24 - 31 cm

Figure 4.12: Horizontal and vertical thin section from Site 1 at the 12th of March. Depth: 24 - 33.5cm.

Figure 4.12 show the ice structure at 24 - 33.5 cm depth. The horizontal cut in figure 4.12a show that the grains are larger than the previous horizontal cut, and the similar color show that the c-axis is oriented in the same direction. The vertical cut show a columnar trend in the ice with a layer of granular ice between the larger columnar grains. The two dark areas in the bottom are brine pockets.

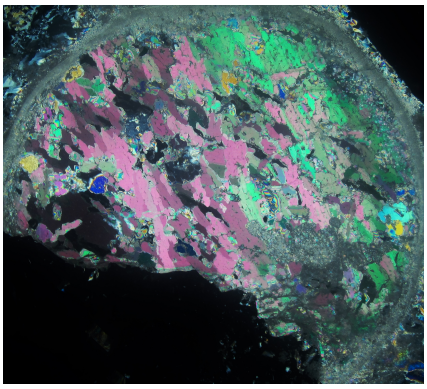

(a) Horizontal cut. 38 - 40cm.

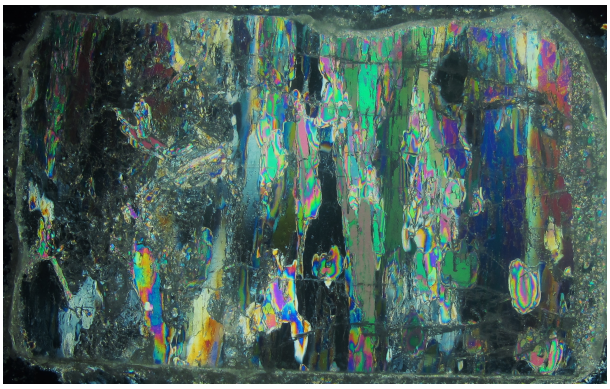

(b) Vertical cut. 33.5 - 38 cm

Figure 4.13: Horizontal and vertical thin section from Site 1 at the 12th of March. Depth: 33.5 - 40cm.

The horizontal cut in figure 4.13 show vaguely the platelets in the columnar ice. In the vertical cut can it be observed smaller grains entrapped in the larger columnar grains. The dark area to the left in the vertical cut is a large brinepocket. There are some irregularties in the area next to the brinepocket.

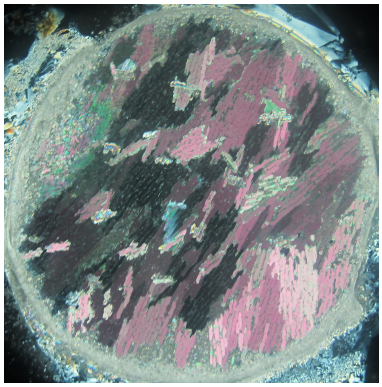

(a) Horizontal cut. 48 - 50cm.

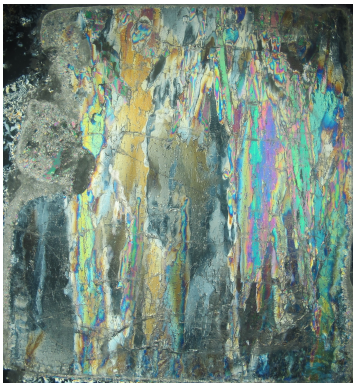

(b) Vertical cut. 40 - 48 cm

Figure 4.14: Horizontal and vertical thin section from Site 1 at the 12th of March. Depth: 40 - 50cm.

Figure 4.14 show the thin section of the bottom layer. The horizontal cut is the lowest 2 cm of the ice sheet. From the color in the horizontal cut can it be seen that the c-axis of the grains is orientated roughly in the same direction. Small brinepockets is trapped between the platelets in the grains. In the vertical cut the ice is mainly columnar with some grains which have been wedged out.

4.4 Salinity

Samples for salinity were collected at both sites at every visit to Svea. The results from Site 1 is presented in figure 4.15 and Site 2 in figure 4.16. The figure show ice depth on the y-axis and bulk

salinity on the x-axis. Each sample is represented by an error bar that extends over the length of the sample. The salinity profiles show a general trend with high salinity at the top and bottom of the ice sheet. This gives the typical c-shape profile through the ice sheet.

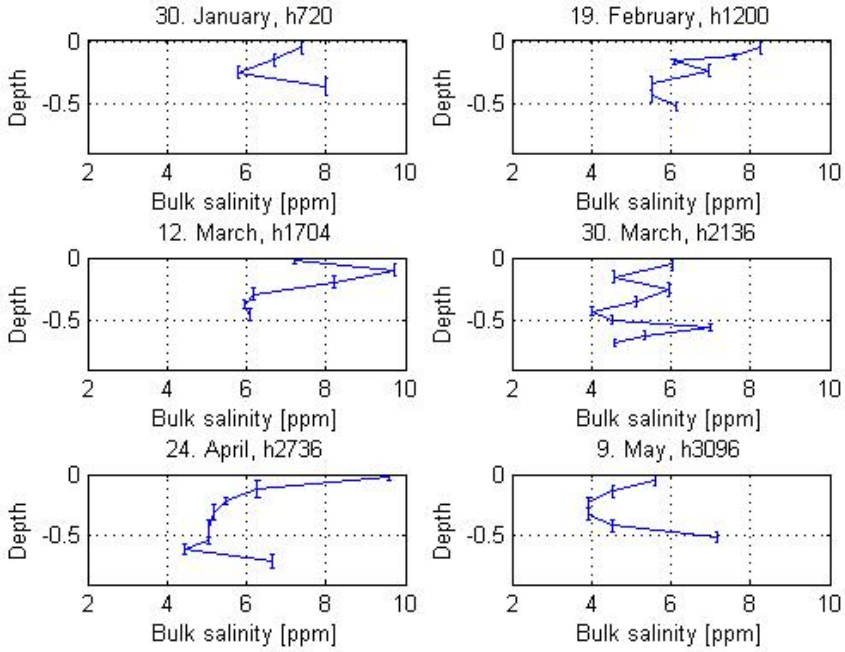

Figure 4.15: Salinity at Site 1.

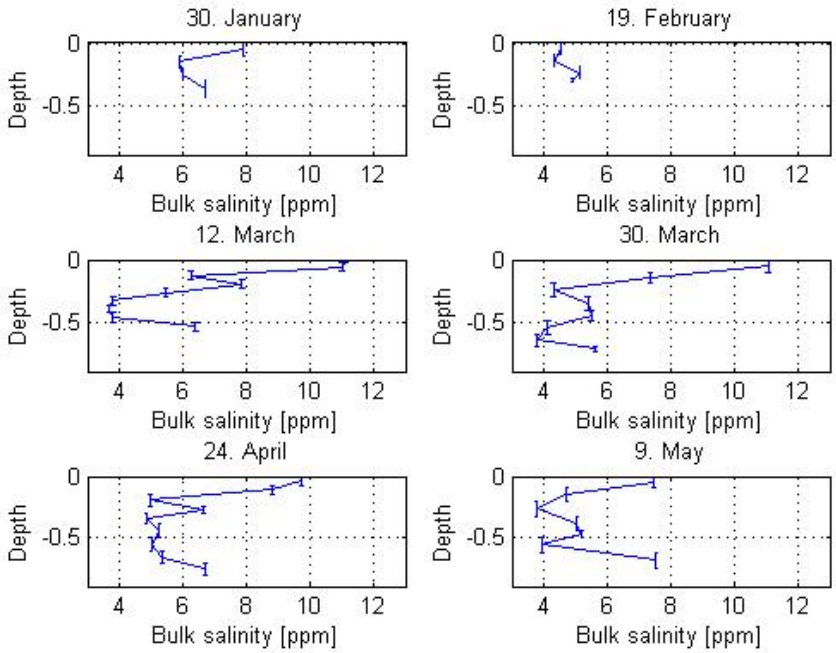

Figure 4.16: Salinity at Site2.

4.5 Density

Density was measured on samples extracted on each visit to Svea. The data from the 30th of January at Site 2 was unfortunantly lost in action during the transportation from Svea to Longyearbyen. The figure show ice depth on the y-axis and density on the x-axis. Each sample is represented by an error bar that extends over the length of the sample. The results is shown in figure 4.17 and 4.18.

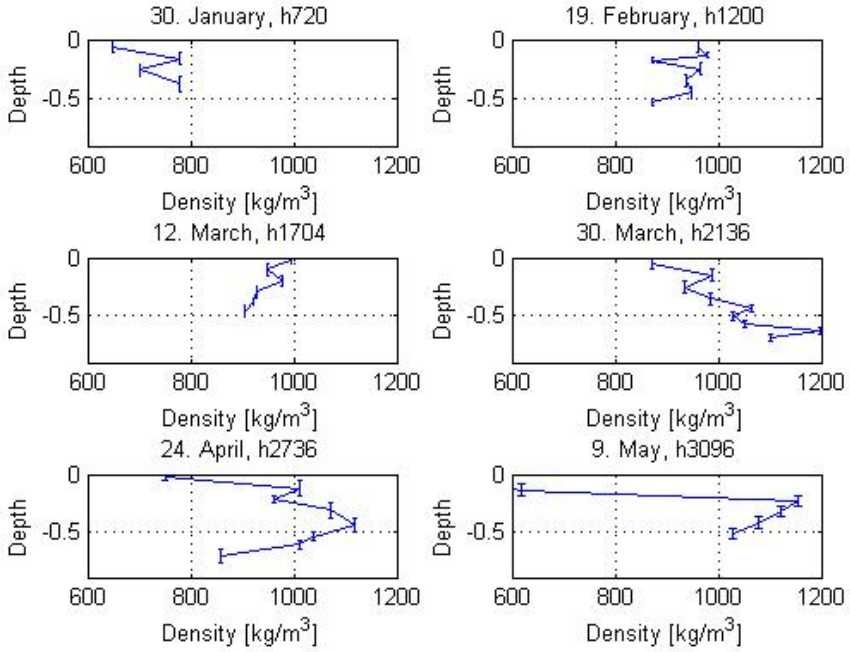

Figure 4.17: Ice density at Site 1.

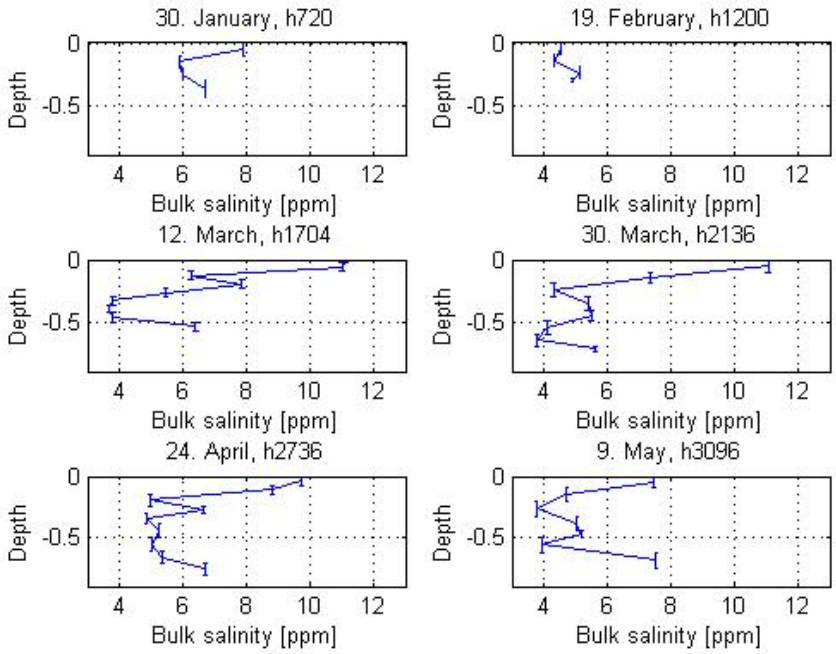

Figure 4.18: Ice density at Site 2.

4.6 Ice thickness, freeboard and snow depth

Table 4.4 show the ice thickness, freeboard and snow depth measured manually at each visit.

Table 4.3: Ice thickness, freeboard and snow depth measured at each visit at both sites.

(a) Site 1

Date	IT [cm]	FB [cm]	SD [cm]
31.01	43	6.5	15
19.02	55	16.5	26
12.03	60	0	19
30.01	64	3	31
24.04	72	0	36
09.05	85	+18	50

(b) Site 2

Date	IT [cm]	FB [cm]	SD [cm]
31.01	44	1.5	7
19.02	33	12	22.5
12.03	65	4	8
30.01	66.5	1.5	25
24.04	78.5	2	22
09.05	77	0	42

Table 4.4: Ice thickness, freeboard and snow depth measured at each visit at both sites.

Compression test was performed on 7 samples retrieved the 2nd of April. The results is presented in Appendix B.

Chapter 5

Analysis and discussion

5.1 General considerations for data acqusition

Van Mijenfjorden has for several years been subject for sea ice investigation. The previous work done on stress measurments in the fjord is the basis for this thesis. The method and instrumentation used in this work is mainly build on experience and knowledge from the earlier campaigns. A difference this year is the use of Geokon Earth Pressure Cells for stress measurments instead of BP stress sensors which have been used earlier. The instrument is basically working in the same manner, but the installation were done slightly different than the BP stress sensors which were installed according to Duckworth & Westermann (1989). During the installation a mechanical chainsaw was used which could be harder to handle than an eletrical one. The slots, where the sensors were installed, got wider than recommended by Duckworth & Westermann (1989), which could reduce the confinement of the sensors. The backfill after the sensors were placed was done with water with the same salinity as the top 20 cm of the ice. It was believed that this would provide a more correct salinity in the backfill than letting seawater refill the slots. To get a more precise angle between the sensors in the rosettes, a wooden stencil was made. This turned out to reduce the time and effort spent on installation.
An error was made when the sensors at Site 2 were configured with LogView. It was not noticed that sensor 3 and 4 was in the range up to 2 MPa, while sensor 1 and 2 were in the range up to 350 KPa. During calibration sensor 3 and for 4 were calibrated to record in MPa, which gave a lower accuracy of the measurments until the error were detected at the reinstallation 30th of March. The accuracy of sensor 3 and 4 from the 30th of January to the 30th of March is 1 KPa. This was believed to be a malfunction in the sensors which led to the extraction of the sensors the 12th of March. In the graphic presentation of the sensors have a smoothing function been used in the data treatment to improve the readability of sensor 3 and 4 in the relevant timespan.
After installation of the sensors at Site 1 the 30th of January, a tidal crack were discovered on the seaside of the sensors. The location of the sensors were supposed to be on the seaside of all tidal cracks, but it was decided to let the sensors stay because the size of the crack was small. At the 12th of March the sensors were moved to the seaside of the crack. A general problem was the event of overwater in February which caused malfunction of the datalogger. The problem could be avoided if all equpiment on the ice were initially elevated from the ice surface. It is also adviced to elevate all

cables from the ice. The 12th of March was spent chopping cables out from the now frozen overwater. Tiltmeters were for the first time applied in this fieldwork and some lessons were learned. During the campaign the tiltmeters were moved in order to lift them from the ice surface to avoid overwater and to adjust the direction of measurment. When the tiltmeters were placed they were orientated with a compass and a GPS with an internal compass. The compass was most likely to close to the tiltmeters so the north needle got disturbed by the metal and showed the wrong direction. This happend 30th of January and the 19th of February. After this a GPS was used to set direction. In addition were the tiltmeters put in different directions during the campaign, it is adviced to have the same direction of both tiltmeters throughout a campaign. A suggestion for installation is to mark the direction before setting down the tiltmeters. If the direction is set as the strait line between two sticks frozen in the ice, then it is easier to maintain correct direction and position.

5.2 Site 1

Site 1 was most affected by the flooding and the results from the 30th of January to 2nd of February is neglected. The analysis and discussion is done in the period from the 1st of March to the 10th of May. Thermistor data was collected and treated by Bård Blæsterdalen in his commenced masterthesis. Air temperature and wind data was retrieved from the Norwegian meteorological office site Norwegian meteorological office (2014). Data for waterpressure was collected and processed by prof. Aleksey Marchenko. All x-axis in the graphs in this section is counting hours from the 1st of January 2014, 00:00. When referred to the x-axis ,the notation is hx e.g. 2200 hours after 1st of January 2014, 00:00, is noted h2200.

Thermal stress

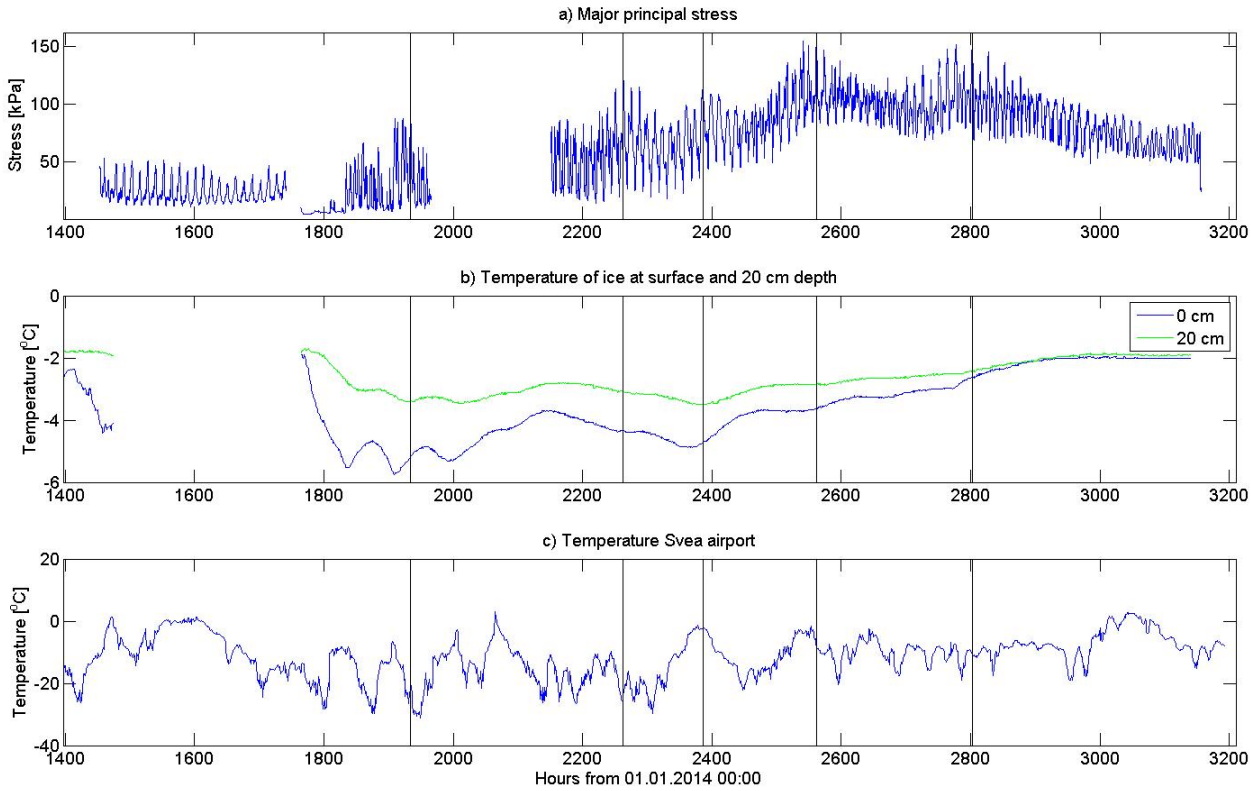

Figure 5.1: Site 1: Stress versus air temperature and temperature at the ice top surface and in 20 cm depth.

Lets first look at the temperature influence to stress. Figure 5.1 show major principal stress (a), temperature at the ice-snow interface and at 20 cm depth (b) and air temperature at Svea airport (c).

Data from 20 cm depth is taken from a closeby thermistor string node at the depth of rosette sensors middle. The five main events is marked with lines in each plot.

Of the five main events, three events occurs simultanously with an increase in the temperatures in figure 5.1b). The three events are event#1 at h1930, event#3 at h2390 and event#5 at h2800. The concurrence between temperature increase and stress development is most obviuos in the temperature at the ice surface, due to the temperature damping through the ice. Key parameters of the relevant events and temperature at the ice surface is shown in table 5.1. Note that the stress in these events are peaking in the very beginning of the temperature increase.

The temperatures in figure 5.1b) is increasing from -4.8°C to -1.9°C in the period between h2360 and h2600. The ice experience in the same period a global increase of stress which diminish towards the end of the period. It would assume that the stress would continue to develop during a temperature increase if the stress was only induced by temperature. However the quite opposite is happening as the stress diminsh in the end of the period.

Event #	σ_{max}	dσ/dt	ΔT	dT/dt
1	93.1 kPa	3.1 kPa/h	0.5°C	+0.026°/h
3	113 kPa	2.1 kPa/h	0.24°C	+0.016°/h
5	162 kPa	1.5 kPa/h	0.4°C	+0.013°/h

Table 5.1: Key parameters for principal stress and temperature at ice surface. dσ/dt is the stress build up, ΔT is the temperature difference during the stress build up, dT/dt is temperature development during the stress build up.

Three of the main stress events occures during an increase in temperature, however the stress peaks is at the very beginning of the temperature increase. In theory should the ice continue the expansion hence generate more stress, but the stress diminsh. The trend can also be seen in the global development. The global stress diminsh while the temperature is further increasing. The same development was observed by Teigen et al. (2005) which indicated that the if the rise in temperature is sufficiently low, creep can develop and relax the stress. Their investigation showed a temperature increase during the stress build up between 0.035 - 0.05° per hour. In this case is the maximum temperature increase in such low rate , 0.026° per hour at the top surface, that the stress induced by temperature could be relaxed by creep. The temperature at 20 cm depth have even less temperature change and a lower rate of temperature increase which would allow creep to develop.Teigen et al. (2005) also suggested that sea ice has an upper limit where it no longer induce stress thermally. Investigations done by Teigen et al. (2005), Prinsenberg et al. (1997) and Moslet (2007) showing that warm ice respond less to temperature changes. The snowdepth was between 31 and 50 cm from h2200 to h3150. The snow is evidently insulating the ice cover so that variations in air temperatur is not affecting the ice in a large extent. The stress generated in the ice is assumed not to be thermally induced due to a large amount of insulating snow which restricts the amount a change in air temperature affects the ice. The change in air temperature is sufficiently damped through the snow cover for creep to develop and relax the thermally induced stress. In addition is it believed that the warm ice respond less to temperature changes.

Stress related to tide

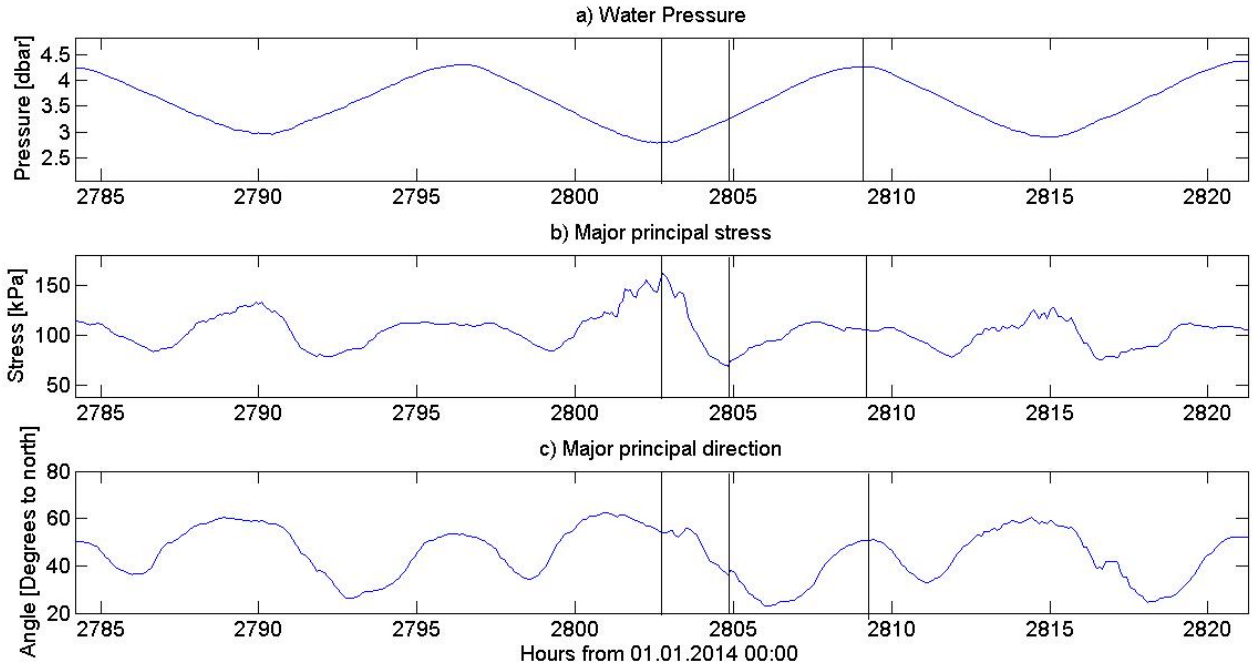

Figure 5.2: Site 1: Principal stress and direction versus tide.

Figure 5.2 show the correlation between tidal cycles (a), represented by water pressure at sea bottom, major principal stress (b) and principal direction (c) for the global maximum principal stress at h2803 $\pm$ 1.5 tidal cycle. This section is representative for the concurrence of tide and principal stress during the campaign. From the graphs there is a clear correlation between pressure and tidal cycles. The correlation is presented with correlation lines in figure 5.2. The stress is having local maximums during both high and low tide, with a local minimum in the intervening period close to mean sea level. The stress generated at low tide is in general higher than the stress generated at high tide. Typically the increase in stress from mean sea level to low tide is $\Delta\sigma_{lowt} = 75$ kPa, and from mean sea level to high tide is the stress increase $\Delta\sigma_{hight} = 40$ kPa. The principal direction in figure 5.2c) correlates with tide. The direction is between 57-62° at low tide, and is slightly turned north during high tide. The stress during high and low tide acts parallell with the last tidal crack at Barryneset. Direction at the intervening period is between 25-36°.

There is a clear correlation between tidal cyclus and stress generated in the ice. This indicates that tide is a driving force for stress generation. The stress developed during low tide can be explained by bending of the landfast ice close to the hinge zone, due to restricted vertical movement in the transition between landfast ice and hinge zone.

It is believed that the landfast ice close to the hinge zone is bend during low tide. The bending is created when the water level drops at low tide and the landfast ice in relation with the hinge zone is restricted to follow the vertical motion. An upward momentum is created in the transition from the

freefloating landfast ice to the landfast ice which interacts with the hinge zone. The ice experience a long term exposure of high stress that allows creep to develop. The scenario is illustrated in 5.3, where Site 1 is located in the transition between the freefloating landfast ice and the hinge zone.

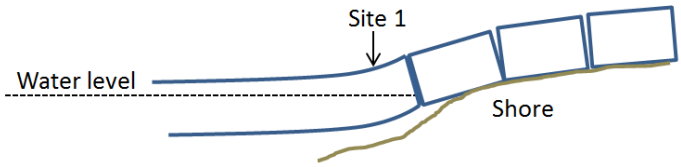

Figure 5.3: Bending in the transition zone between the hinge zone and the freefloating landfast ice at low tide. The long term exposure of high stress allows creep to develop.

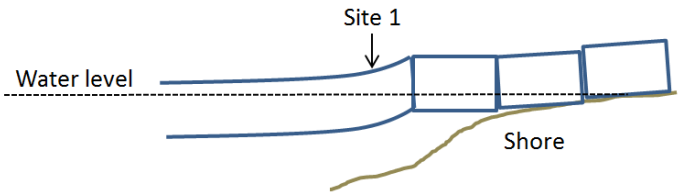

Figure 5.4: Permanently change of the geometry of the transistion zone (Site 1) due to creep.

Bending of the ice sheet would create higher stresses in the top part of the ice, which would be reduced further down in the icepack. When looking at the difference between sensor 1 and 4 it can be seen in figure 5.5 that sensor 4 experience higher stresses than sensor 1. Sensor 4 is here installed at 12.5 cm depth and sensor 1 at 20 cm depth. The higher stress at sensor 4 show that the stress is higher in the top part of the ice. Since the thermal expansion is believed to not contribute to stress generation, it would suppose that higher stress in the upper part of the ice is due to bending.

In a situation where bending was the only process affecting the ice, the difference between sensor 1 and 4 would be greatest during low tide, where the bending is created. This is however not happening in this case. Figure 5.5 show that the difference between sensor 1 and 4 is largest at high tide. The difference at low tide is 35 kPa and at high tide 65 kPa. These values vary some at each cycle, but it show the magnitude of the difference between the two sensors. Sensor 1 reads high stress during low tide, and low stress at high tide. This supports that the ice experience bending during low tide. Because of the high readings in sensor 4 at high tide would it assume that another mechanism is generating stress in the top layer of the ice.

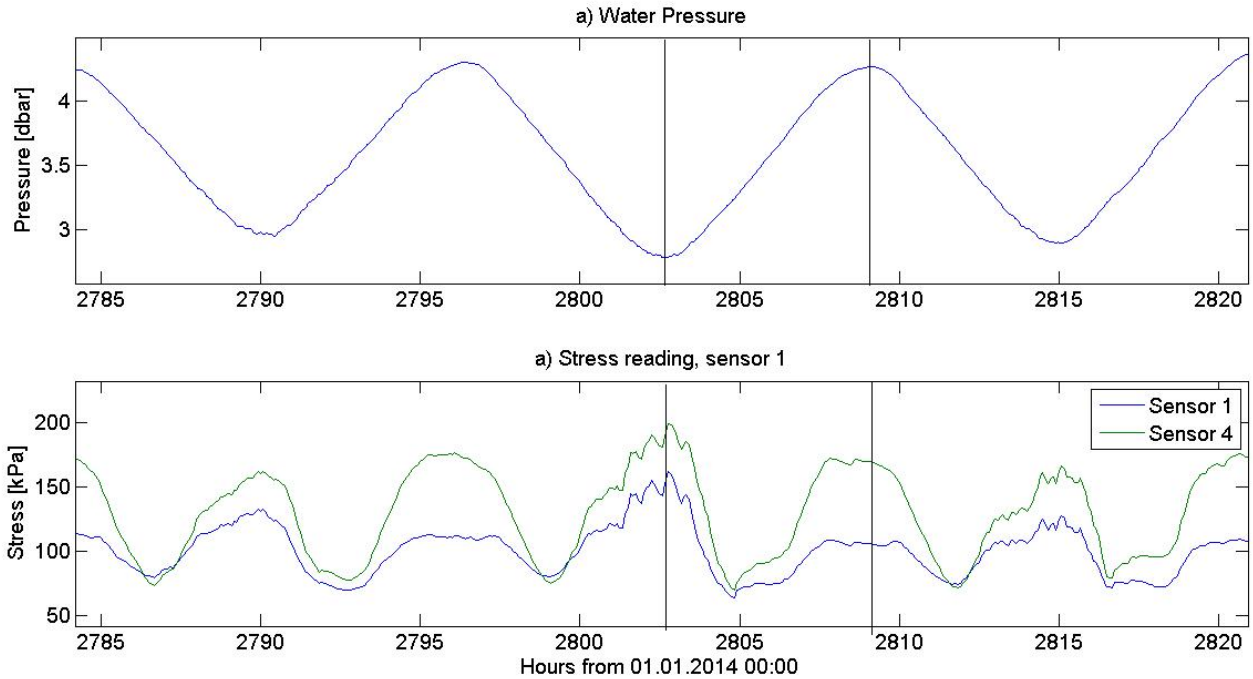

Figure 5.5: Water pressure correlation with sensor 1 and sensor 4.

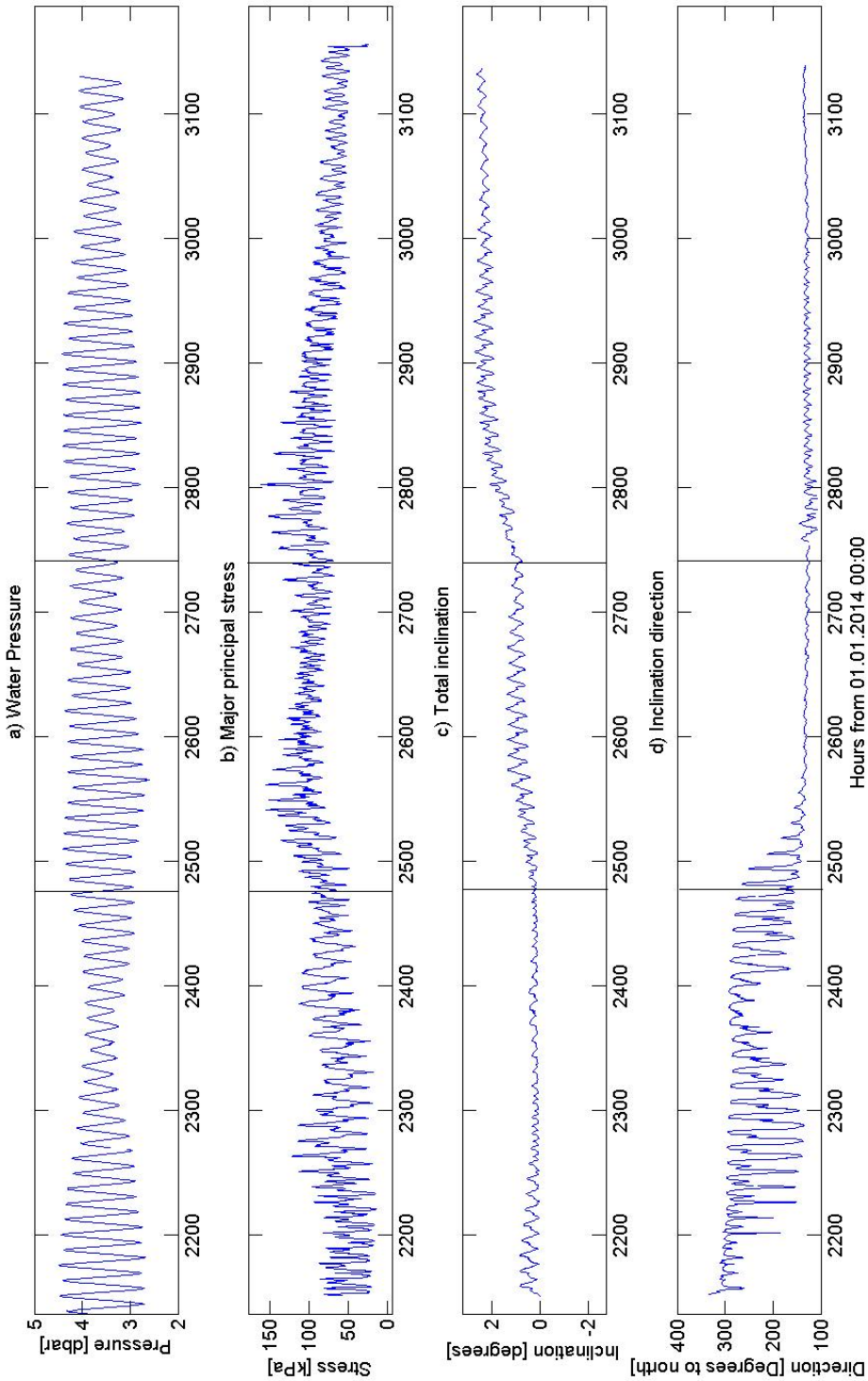

Figure 5.6: Inclination and direction versus principal stress and water pressure. Increase in tidal range correlates with change in inclination and increase of stress (marked with lines).

Inclination of Site 1 is increasing through the season. Inclination is seen in context with tide in figure 5.6. It shows that the inclination is increasing when the tidal range (differance between high tide and low tide) is increasing. The correlation may explain how the ice is bend during an increase in tidal amplitude. Bending may develop in the transition between free floating landfast ice and the landfast ice boundary during low tide. The boundary is connected to the hinge zone by freezing or pressure and shear strength. When the tidal range is increasing, the difference between the landfast ice boundary and the free floating landfast ice increase, which gives a higher upward momentum in the transition zone at each tidal cycle. The tidal cycle is believed to act sufficiently slow for creep to develop, and the transition zone is permanently bend. The transition zone will experience more bending at each tidal cycle as the tidal range increase. When the tidal range decrease the inclination is permanently changed, but the forces are not sufficient to create more bending. The next period with increasing tidal range is again affecting the transition zone and a new process of creep occurs and increase the inclination. The two events of increasing inclination is occuring simoultanious as a stress build up in the ice. It would reasonable to assume that the stress build up is caused by bending hence compression of the top layer of the ice. The direction of the inclination is stabilized when the inclination increase. This can be explained by creep which has permanently changed the geometry of the ice in the transition zone. The direction is stabilized to 130°. The inclination is not fluctuating anymore, but is constant tilting against the sea perpindicular to Barryneset.

The correlation between tide, pressure and inclination is shown in figure 5.7. The section shown is during the global maximun stress at h2803. The ice is having most inclination during low tide, which supports the argument of bending during low tide. In addition is inclination and stress increasing during high tide. It would require more investigation to clarify this behaviour.

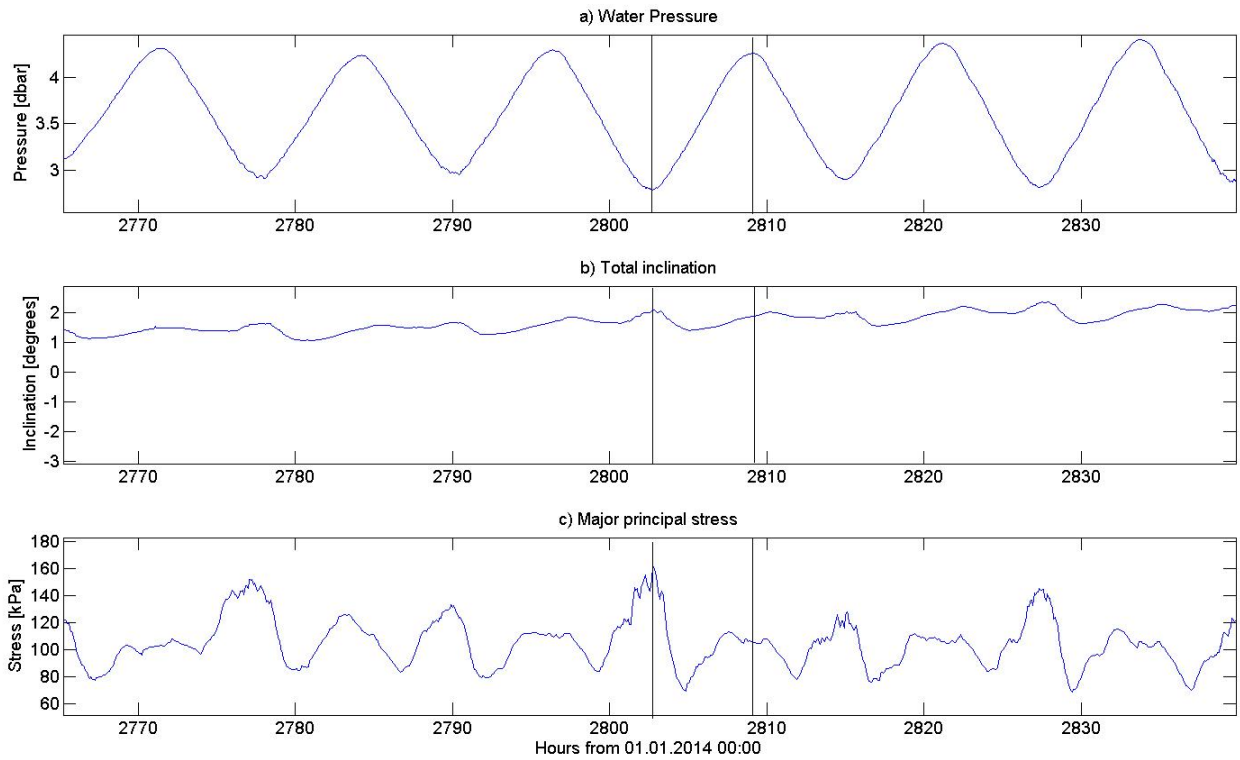

Figure 5.7: Inclination versus principal stress and water pressure. Increase in tidal range correlates with change in inclination (marked with lines).

The direction of the principal stress is acting parallell with the last tidal crack at Barryneset. This can be explained by looking at the shape of the shore in Sveasundet. The strait is short and narrow with basins on each side. Braganzavågen to the west and Sveabukta to the east. Two headlands is penetrating the strait from north and south, which reduce the width of Sveasundet to about 1/4 of the basins width. The stress induced in the two basins are concentrated around the two headlands, similar to when stress is concentrated around a hole in a pressure plate. The stress can not be transferred through the headland, and it accumulates around the headland, as shown in figure 5.8. The accumulation of stress will increase the stress around Barryneset. This process may explain the direction of the main principal stress.

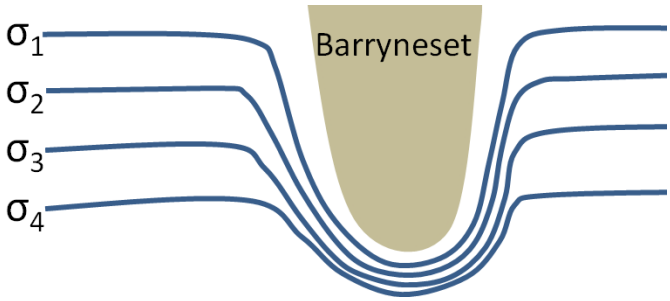

Figure 5.8: Stress in Braganzavågen and Sveasundet is concentrated when reaching the natural boundary of Barryneset.

Figure 5.9 show the rearrangement of the hinge zone from low tide to high tide. At low tide the ice blocks is either stranded or being randomly orientated which decrease the horizontal span of the hinge zone. At high tide the ice blocks is put in a fixed order. The horizontal span of the hinge zone is increased, but can not expand. The extension of the hinge zone creates stress when the confinement of the ice wont allow expansion. This may explain the stress developed during high tide. However this will not explain the change in inclination during high tide. It could be observed reorganization of the hinge zone during low and high tide during the visits to the site. Local factors such as rocks, ice rubble and variations in the ground which interacts with the hinge zone is affecting the organization of the hinge zone.

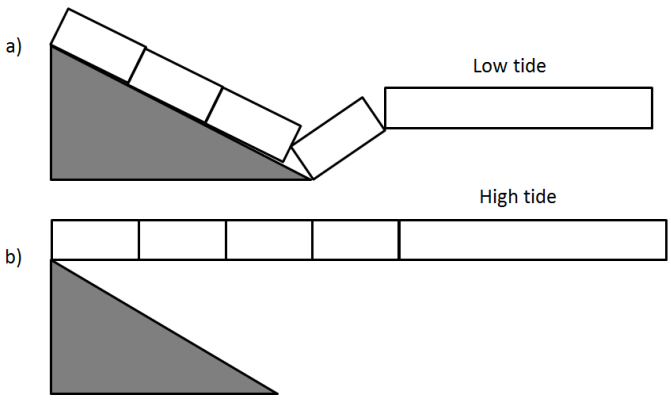

Figure 5.9: Stress developed during high tide by ice blocks moved into a fixed order. At high tide the span of the hinge zone is increased, but is confined by the shore. The confinement create stress in the ice as it wish to expand.

5.3 Site 2

Stress related to temperature

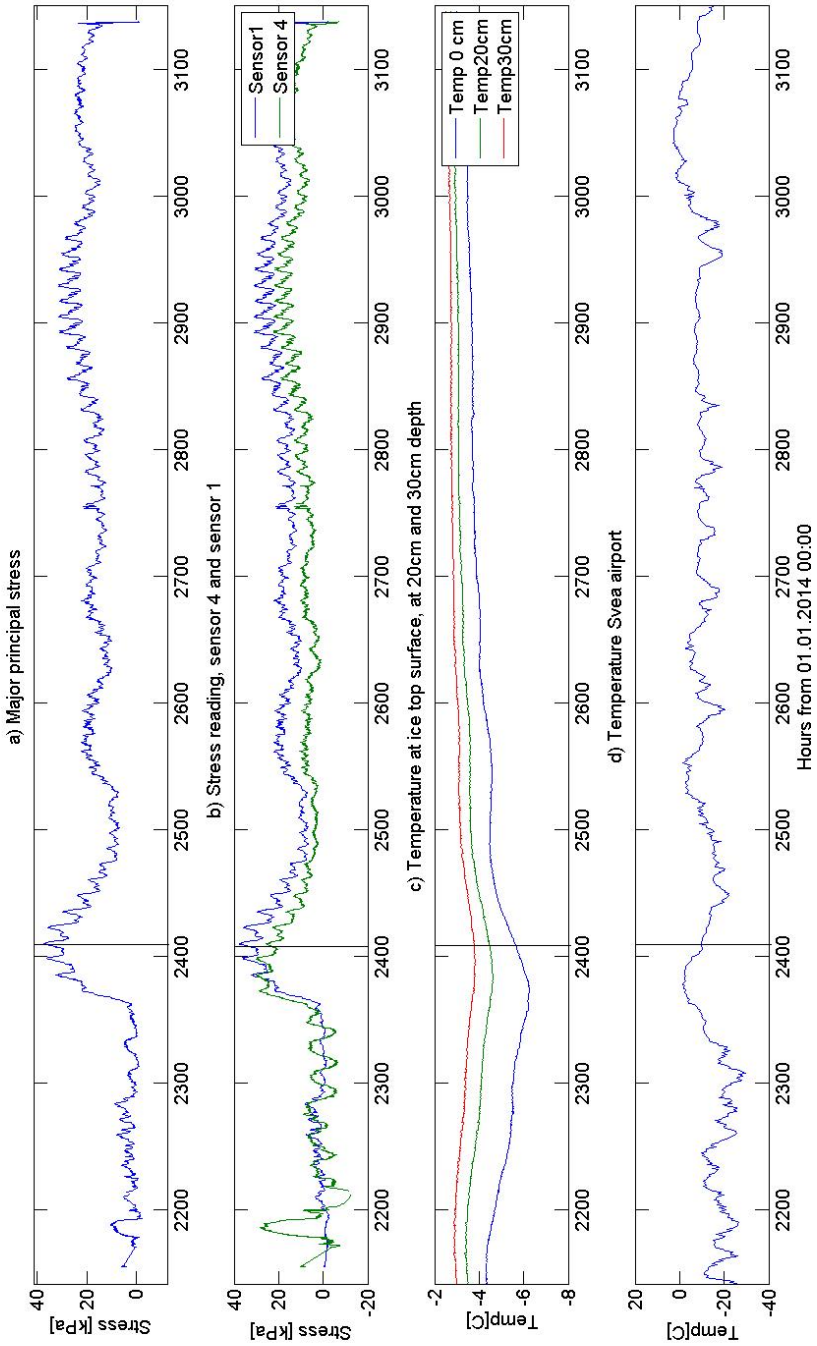

Figure 5.10: Major and minor principal stress versus temperature in the ice and air temperature.

At Site 1 it was argued that there is not any particular thermal stress because of the long term increase in temperature and the thick snowcover. At Site 2 the snow cover was about 10 cm less, which leaves the ice more exposed to temperature change in the air.
Figure 5.10 show the major principal stress (a), stress reading of sensor 1 and sensor 4 (b), temperature at the ice surface, at 20 cm depth and 30 cm depth (c) and airtemperature (d). The correlation lines show a correlation between the ice surface temperature and the major stress development. The figure show that the temperature increase in the ice (c) is correlating with the stress in one event; h2410. At h2410 the major stress build up is $\Delta\sigma_{h2410} = 1.3$ kPa/h when the temperature increase in the same period is $\Delta T_{h2410} = 0.02$°C/h. Compared with the temperature increase in Teigen et al. (2005) between 0.035°C/h - 0.05°C/h, the temperature increase of 0.02°C/h is lower, but the correlation of stress and temperature show that it is likely that the stress peak is due to thermal expansion.

Barrault & Høyland (2007) derive a model which could determine the freeboard based on ice thickness and snowdepth. If one assumes constant values for ρ_{water}, ρ_{ice} and ρ_{snow} the freeboard can be estimated. In this case the ice thickness and snow depth were measured before and after the three main events mentioned earlier. Since the temperature was sub-zero during this period it would assume that there was no major changes in the snow cover and ice thickness. When taking the average value of snow depth and ice thickness, the model estimates a freeboard of 0.01 m. From this it is reasonable to believe that the ice have been flooded this period. Further is the salinity measured at the 24th of April showing high salinity in the top layer of the ice. This indicates strongly that the ice have been flooded in the period between h2370 and h2500. The increase of top surface temperature while the air temperature decrease suggest that the ice have been flooded during this period. The flooding can cause a rapidly temperature increase at the top surface of the ice, but the temperature increase in this period is rather low. The temperature increase at the top surface of the ice at event h2410 could be caused by flooding of the ice.

Stress related to tide

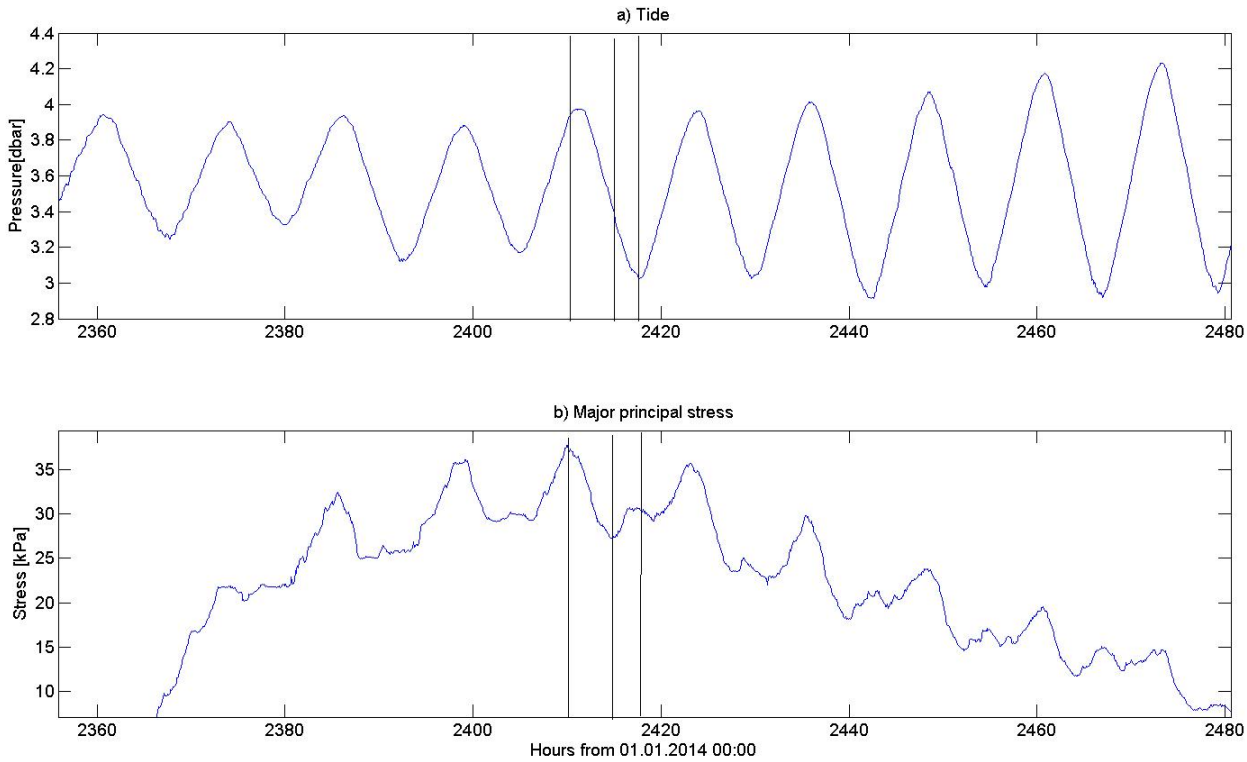

Figure 5.11: Major and minor principal stress versus water pressure.

5.11 show the water pressure during the tidal cycles and the global main event of the principal stress at h2410. The figure shoe a clear correlation between stress and tide. The stress is peaking at high tide but is stable at low tide. The difference between the stress at high and low tide is in the range of 6 - 8 kPa. A difference between Site 2 and Site 1 is the diminshing stress during low tide at Site 2 while the stress was increasing during low tide at Site 1. This indicates that the ice close to shore is far more exposed to stress which is not transferred further out on level ice. This could be explained by cracks between the sites or brine channels and brine pockets which absorb the stress. Gabrielsen et al. (2008) suggest when the load is applied at a slow rate, where the time constant is larger than 1 hour such as a tidal cyclus, then the maximum value of the stress is highly dependent on the viscous properties of the ice.

A mechanism which can explain the correlation between tide and stress is flexural bending during flooding at high tide. If one consider that the ice is fastend to shore and is subjected to flooding. Lets further assume that the ice is not perfectly flat at the top surface, but will feature an uneven surface with small depressions. The added water will then congregate in these depressions. This will add weigth at one area of the ice, and leaving another area free of water. The pits where water is gathered will have a reduced bouncy, because of higher density of water than ice, and the ice will bend

causing compression in the upper layer of the ice. It could also be assumed that the whole icesheet is depressed when the boundary is fastend, which create flexural bending of the entire landfast ice during flooding. The stress in figure 5.11 show that the stress is reaching local minimum when the tide is reaching mean sea level. At this point the water level is sufficiently low for the flooded water to be drained out. The extra weight on the ice is then expelled and the ice gain bouancy. As the ice which was mostly affected by flooding is recovering boyancy, the bending gets less and the stress is diminishing.
The principal direction is having big fluctuations until the global rise in stress. When the stress is increasing globally at h2360 then the direction is stabilized to 45° - 55° to north. This bearing is the same as the direction of the distance from shore to shore crossing Site 2. The strech goes from Skanerodden southwest of Site 2 to Nordbekken northwest of Site 2. This agrees with the model proposed by Teigen et al. (2005) regarding partly confined thermal expansion. This correlates also with the increase in air temperature during the main events at h2400, h2575 and 2675 which could have been the driving force of thermal expansion in the top layer. However the longest distance from shore to shore crossing Site 2 is at bearing 65° - 75° to north and the major principal direction should be in this direction according to theory. In addition is it believed that thermal expansion did not create any significant stress in the ice. Note that the direction of minor principal stress is where the distance from shore to shore is shortest. The direction of major principal stress is in the same range as Site 1, which was 57°-62° to north. This could be caused by the stress consentration around Barryneset. The stress consentration at Barryneset could affect the direction at Site 2 through propagation of stress, or that the stress consentration reach further out in the strait to Site 2.

Stress related to wind

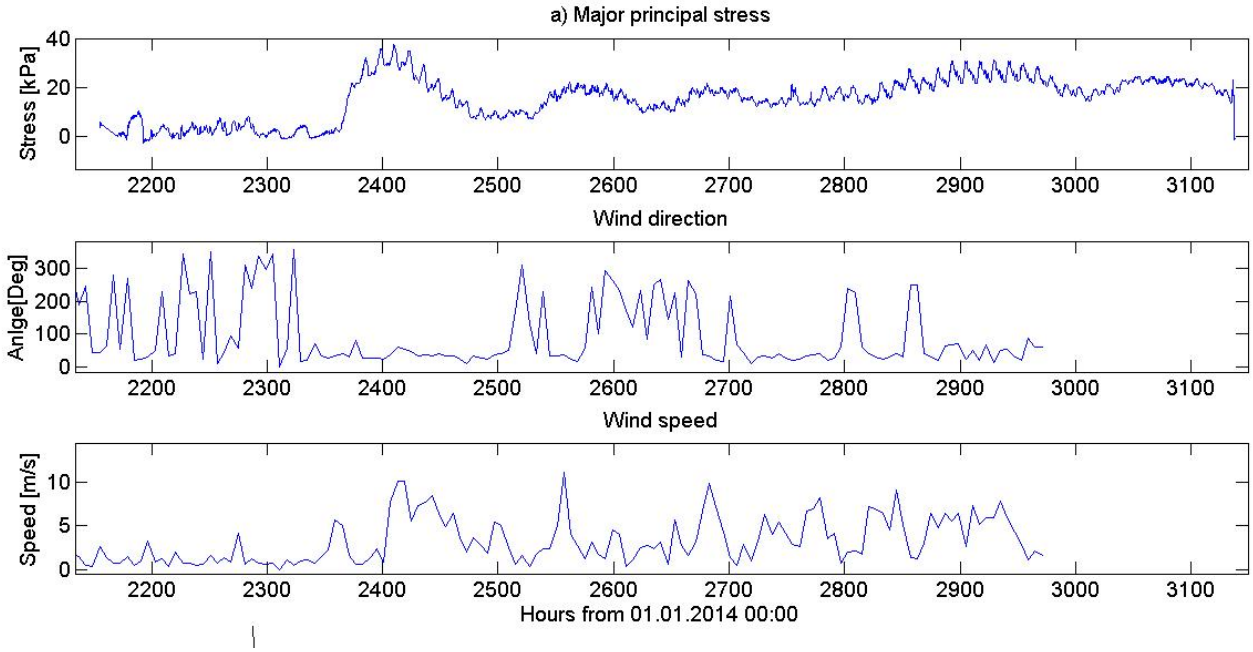

Figure 5.12: Principal stress versus wind speed and direction.

Teigen et al. (2005) argue that wind can, in theory, generate stress under the right circumstances. The circumstances mean that the wind direction is going straight into the fjord and the wind speed must be sufficiently high, probably above 20 m/s. 5.12 show the wind speed and direction together with major principal stress. For the wind to get maximum fetch of the ice gathered in the main basin of Van Mijenfjorden, the direction must be between 240° and 250° to north. In Sveasundet is the situation different. Due to the topography around Sveabukta, the direction of maximum fetch is between 205° and 210°, where the fetch is about 10 km. It can not be found any correlation between stress and wind regarding the circumstances needed for stress generation.

5.4 Salinity

The salinity can be seen in context with temperature because salinity and temperature is closely related. The salinity profile from the 30th of January show a typical c-shape. Salt is efficiently trapped in the fast growing initial ice. As the ice continue to grow downwards, the growth process is slowed down and salt is expelled from the ice. The salinity is bigger towards the bottom due to brine migration towards the bottom surface of the ice. Between the 30th of January and the 19th of February the ice was flooded and the overwater was 20 cm at February the 19th. The salinity on trip no 2 showed an increase in the salinity at the top surface. This could possibly be due to the flooding where ice have been formed on the top surface, but it could also be caused by a negative temperature gradient which trigger the brine to migrate upward in the ice. The negative temperature gradient might be

established when the air temperature was steady at 4° during 24 hours the 11th of February.
The salinity profile the 12th of march show high salinity in the topmost 12 cm which is due to the newly formed ice on top. Overwater from the flooding was frozen and the ice had grown 20 cm on the prevoius top surface, but the ice thickness was in total only 5 cm thicker. This could be due to melting of top surface or melting at the bottom surface. Melting of the bottom surface can be explained by the heat transport during the event. When water is flooding the ice the heat transport out of the added water will start immediatly after coming in contact with colder surroundings according to the second law of thermodynamics. The initial ice is now insulated from the cold air temperature by the water which change the thermal regime in the cover. The temperature gradient in the inital ice is now not existing because the temperature at the top surface and bottom surface is equal: at the freezing point of sea water. The heat from the initial ice will not transport any heat towards the top surface until the overwater is fully frozen. The heat flux from the ocean is no longer transported through the ice cover to colder temperatures, but rather melting the ice from underneath. When the overwater is fully frozen, then the thermal gradient can be reestablished and the heat flux from the ocean is again transported through the ice cover.

5.5 Ice texture

The ice texture was found to be granular down to 31 cm. The first 20 cm is the newly formed ice and should be granular do to rapid growth, the next 10 cm is the initial top surface which also is granular. The granular grains is growing in depth with some development of columnar grains. The grains is getting more columnar in shape as the depth reach 31 cm, however this is not clearly seen. At 31 cm depth there is still granluar ice, with some columnar development. Further down to 40 cm the length of the columnar grains has increased. There were grains which were wedged out in the compatetive growth, showing that the vertical c-axis was not fully developed. At 50 cm the grains are larger and small brinepockets is trapped between the platelets. The grains has roughly the same orientation of the c-axis, which is interpretated as C-3 ice. The C-3 ice indicates that the currents close to Barryneset is steady at one direction. This correlates good with the theory given by Sanderson (1988).

Chapter 6

Conclusions

Stress measurments in first-year sea ice in Sveasundet in the Van Mijenfjorden, Svalbard were performed during the winter 2014. The measurments were conducted at two sites: close to a hinge zone (Site 1) and 200 meters out in Sveasundet (Site 2). In addition were inclination of the ice observed at both sites through the season. The basic conclusions are as follows.

- Maximum principal stress at Site 1 was measured to 162 kPa at the 26th of April. The maximum principal stress at Site 2 was 37.7 kPa at the 10th of April. The principal stress was significant lower at Site 2 through the season.
- Stress at both sites correlates well with tide. Highest stress was recorded during low tide at Site 1, and during high tide at Site 2.
- Bending of the ice close to the hinge zone generated stress at Site 1. The bending increased through the season when the tidal range increased.
- Temperature was of less importance to stress generation at Site 1. The ice was covered with snow up to 50 cm.
- The event of maximum stress at Site 2 was contributed by flooding and the following thermal expansion.
- Direction of major stress at Site 1 was parallell with the shore at Barryneset.
- Direction of minor stress at Site 2 was where the distance to the shore was shortest.

Bibliography

Barrault, S. & Høyland, K. V. (2007), Mechanisms and measurments of stresses in first-year landfast ice, *in* 'POAC '07: recent development of offshore egnieering in cold regions. Proceedings of 19th International Conference on Port and Ocean Engineering under Arctic Conditions, Dalian, China: Dalian University of Technology Press', Vol. 2, pp. 685–694.

Bergdahl, L. (1977), *Physics of ice and snow as affects thermal pressure*, Gøteborg: Chalmers University of Technology.

Caline, F. & Barrault, S. (2008), Transmission of level stresses to ice foot through a tidal crack, *in* 'Proceedings of 19th IAHR International Symposium in Ice, Vancouver, BC', Vol. 2, International Association of Hydraulic Engineering and Research, pp. 831–840.

Duckworth, R. & Westermann, P. (1989), 'Stress and strain instruments developed for field measurment of ice', *IEEE Journal of Oceanic Engineering* **14(2)**, 159–165.

Ellingsen, S. (2006), Stresses in first year sea ice, Master's thesis, Norwegian University of Science and Technology, Trondheim, Norway.

Gabrielsen, M., Barrault, S., Caline, F. & Høyland, K. V. (2008), Comparison of physical and mechanical properties of coastal ice and level ice, *in* 'Proceedings of 19th IAHR International Symposium in Ice, Vancouver, BC', Vol. 2, International Association of Hydraulic Engineering and Research, pp. 956–974.

Geokon (2011), *Instruction manual. Models 4800, 4810, 4815, 4820 and 4830. VW Earth Pressure Cells.*

Høyland, K. V. (2013), 'Lecture compendium in tba4265 arctic and marine civil engineering, Norwegian University of Science and Technology'.

Kovacs, A. (1996), 'Sea ice part 1. bulk salinity ice floe thickness', *Cold Regions Research and Engineering Laboratory, CRREL Report 96-7* .

Moslet, P. O. (2001), Estimation of loads exerted by sea ice on the quay at kapp amsterdam, the van mijeen fjord, Master's thesis, Norwegian University of Science and Technology, Trondheim, Norway.

Moslet, P. O. (2007), In-situ measurments of sea-ice parameters that affect the ice loads on coastal and offshore structures, PhD thesis, Norwegian University of Science and Technology, Trondheim, Norway.

Moslet, P. O. & Høyland, K. V. (2003), Ice stress measurments adjacent to a wide structure in landfast ice, *in* 'Proceedings of 17th International Conference on Port and Ocean Engineering under Arctic Conditions, Trondheim, Norway'.

Nakawo, M. & Sinha, N. (1984), 'A note on brine layer spacing first year', *Atmosphere-ocean 22* **2**, 193 – 206.

Norwegian meteorological office (2014).
URL: *www.eklima.no (obtained: 4th of May 2014)*

Østerås, E., Finseth, J. & Høyland, K. V. (2011), Ice action on a geobank embankment in landfast sea ice on svalbard, *in* 'Proceedings of 21th International Conference on Port and Ocean Engineering under Arctic Conditions, Montrèal, Canada'.

Prinsenberg, S., Fowler, G., van der Baaren, A. & Beanlands, B. (1997), 'Ice stress measurments from landfast ice going from landfast ice along canda's labrador coas', *Cold Regions Science and Technology* **25**, 1–15.

Sanderson, T. (1984), Thermal forces against isolated structures, *in* 'IAHR Ice Symposium Conference, Hamburg, Germany', Vol. 3, pp. 543–546.

Sanderson, T. (1988), *Ice mechanics - risks to tooshore structures*, BP Petroleum Development Ltd. London: Graham and Trotman.

Teigen, S. H., Høyland, K. V. & Moslet, P. O. (2005), Thermal stresses in first year sea ice, *in* 'Proceedings of 18th International Conference on Port and Ocean Engineering under Arctic Conditions, Potsdam, NY: Clarkson University', Vol. 2, pp. 893–903.

The Norwegian Institute of polar research (2014).
URL: *http://www.npolar.no/no/tjenester/kart/ (obtained: 19th of May 2014)*

Appendix A

MSc Thesis Template

MASTER DEGREE THESIS

Spring 2014
for

Student: Carl Magnus Vindegg

Stress measurments in landfast sea ice in Van Mijenfjorden in Svalbard.

BACKGROUND

The arctic seas are expecting increased activity due to northern ship lanes and findings of hydro carbon resources. The increased activity requires construction of coastal facilities and structures. In the winter time is sea ice a feature which must be accounted for in the design of the structure. Sea ice is a material which is not fully understood, and it is necessary to understand the behavior of sea ice in order to operate in a safe and effective manner in ice infested waters.

TASK

A fieldwork will be conducted winter 2014 which will consist of measurements of internal stress in the ice, inclination of the ice and retrieve ice core samples for more thorough investigation of the ice. The hinge zone will be profiled to observe the movement during high tide and low tide.

Task description

The fieldwork will be conducted in Van Mijenfjorden, Svalbard. The work will last from late January to mid May. The investigation site will be visited several times during the winter for data collection, retrieval of ice core samples and hinge zone profiling.

Objective and purpose

The main objective of the fieldwork is to register internal stress and find in which degree this correlates with temperature, tide, ice movement and wind.

General about content, work and presentation

The text for the master thesis is meant as a framework for the work of the candidate. Adjustments might be done as the work progresses. Tentative changes must be done in cooperation and agreement with the professor in charge at the Department.

In the evaluation thoroughness in the work will be emphasized, as will be documentation of independence in assessments and conclusions. Furthermore the presentation (report) should be well organized and edited; providing clear, precise and orderly descriptions without being unnecessary voluminous.

The report shall include:

- Standard report front page (from DAIM, http://daim.idi.ntnu.no/)
- Title page with abstract and keywords.(template on: http://www.ntnu.no/bat/skjemabank)
- Preface
- Summary and acknowledgement. The summary shall include the objectives of the work, explain how the work has been conducted, present the main results achieved and give the main conclusions of the work.
- The main text.
- Text of the Thesis (these pages) signed by professor in charge as Attachment 1.

The thesis can as an alternative be made as a scientific article for international publication, when this is agreed upon by the Professor in charge. Such a report will include the same points as given above, but where the main text includes both the scientific article and a process report.

Advice and guidelines for writing of the report is given in "Writing Reports" by Øivind Arntsen, and in the departments "Råd og retningslinjer for rapportskriving ved prosjekt og masteroppgave" (In Norwegian) located at http://www.ntnu.no/bat/studier/oppgaver.

Submission procedure

Procedures relating to the submission of the thesis are described in DAIM (http://daim.idi.ntnu.no/). Printing of the thesis is ordered through DAIM directly to Skipnes Printing delivering the printed paper to the department office 2-4 days later. The department will pay for 3 copies, of which the institute retains two copies. Additional copies must be paid for by the candidate / external partner.

On submission of the thesis the candidate shall submit a CD with the paper in digital form in pdf and Word version, the underlying material (such as data collection) in digital form (e.g. Excel). Students must submit the submission form (from DAIM) where both the Ark-Bibl in SBI and Public Services (Building Safety) of SB II has signed the form. The submission form including the appropriate signatures must be signed by the department office before the form is delivered Faculty Office.

Documentation collected during the work, with support from the Department, shall be handed in to the Department together with the report.

According to the current laws and regulations at NTNU, the report is the property of NTNU. The report and associated results can only be used following approval from NTNU (and external cooperation partner if applicable). The Department has the right to make use of the results from the work as if conducted by a Department employee, as long as other arrangements are not agreed upon beforehand.

Tentative agreement on external supervision, work outside NTNU, economic support etc.
Separate description is to be developed, if and when applicable. See http://www.ntnu.no/bat/skjemabank for agreement forms.

Health, environment and safety (HSE) http://www.ntnu.edu/hse
NTNU emphasizes the safety for the individual employee and student. The individual safety shall be in the forefront and no one shall take unnecessary chances in carrying out the work. In particular, if the student is to participate in field work, visits, field courses, excursions etc. during the Master Thesis work, he/she shall make himself/herself familiar with "Fieldwork HSE Guidelines". The document is found on the NTNU HMS-pages at http://www.ntnu.no/hms/retningslinjer/HMSR07E.pdf

The students do not have a full insurance coverage as a student at NTNU. If you as a student want the same insurance coverage as the employees at the university, you must take out individual travel and personal injury insurance.

Startup and submission deadlines
Startup and submission deadlines are according t o information found in DAIM.

Professor in charge: Amund Bruland

Other supervisors: Aleksey Marchenko

Department of Civil and Transport Engineering, NTNU
Date: 06.01.2014, (revised: 21.06.2014)

_____
Professor in charge (signature)

Appendix B

Results of compression test

Compression test was performed on 7 ice core samples retrieved the 2nd of April. The depth of the samples is from the top surface and down. The results are shown in figure 1.

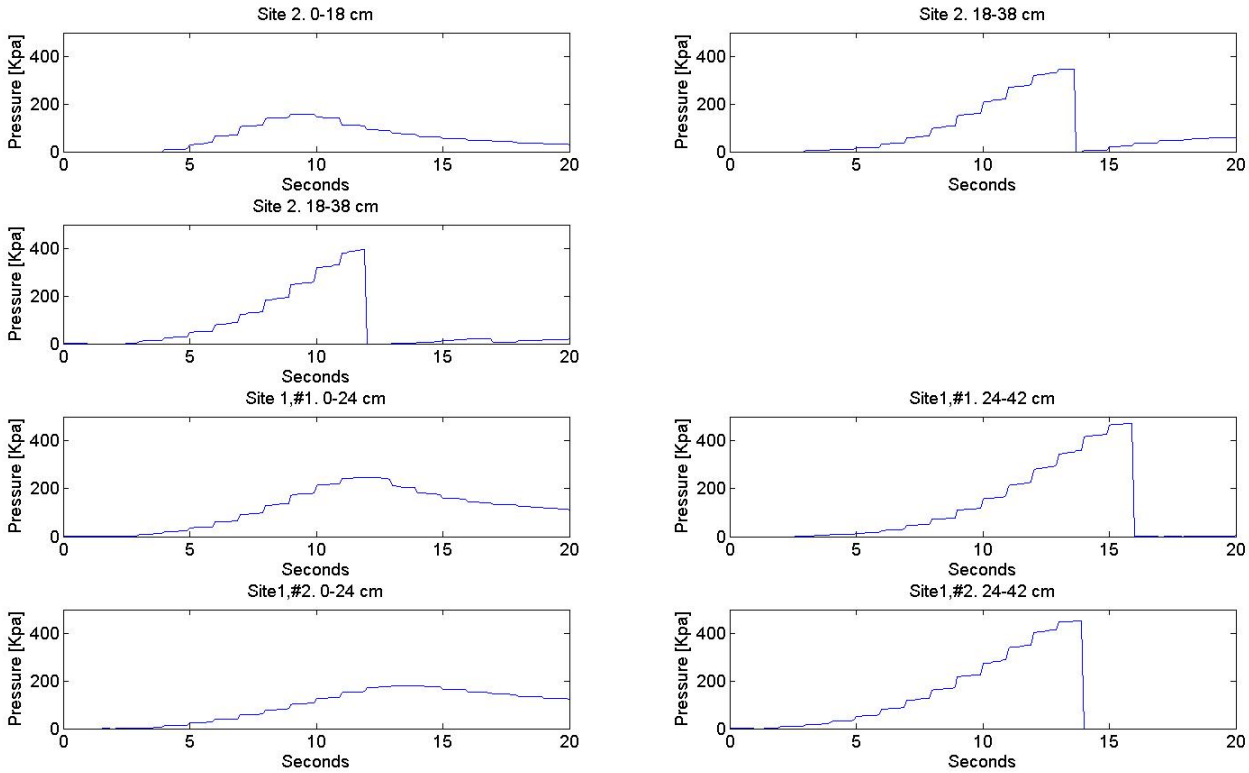

Figure 1: Compression test performed on 7 samples from both Site 1 and Site 2.